A coupled MPM-DEM method for modelling soil-rock mixtures

Li, Jianguo; Wang, Bin; Wang, Di; Zhang, Pei; Vardon, Philip J.

DOI
10.1016/j.compgeo.2023.105508

Publication date
2023

Document Version
Final published version

Published in
Computers and Geotechnics

Computers and Geotechnics 160 (2023) 105508

Contents lists available at ScienceDirect

Computers and Geotechnics

journal homepage: www.elsevier.com/locate/compgeo

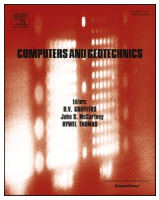

A coupled MPM-DEM method for modelling soil-rock mixtures

Jianguo Li [a,b], Bin Wang [a,*], Di Wang [a,*], Pei Zhang [c], Philip.J Vardon [d]

[a] State Key Laboratory of Geomechanics and Geotechnical Engineering, Institute of Rock and Soil Mechanics, Chinese Academy of Sciences, Wuhan 430071, Hubei, China
[b] University of Chinese Academy of Sciences, Beijing 100049, China
[c] Key Laboratory of Coastal Environment and Resources of Zhejiang Province, School of Engineering, Westlake University, Hangzhou 310024, Zhejiang Province, China
[d] Section of Geo-Engineering, Delft University of Technology, 2628CN Delft, the Netherlands

ARTICLE INFO

Keywords:
Material point method
Discrete element method
Binary granular mixture
Soil-rock mixture
Triaxial test

ABSTRACT

Aiming at modelling the mechanical behaviour of soil-rock mixtures accurately and efficiently, a coupled MPM-DEM formulation combining the material point method (MPM) and the discrete element method (DEM) is proposed. It is solved concurrently via the contact force linking the two individual methods. Specifically, the soil is modelled with MPM as continuums to avoid handling the contacts between fine particles. The rocks are modelled by DEM to capture the contact characteristics of rocks. This method is validated with ball impacting and block sliding tests first for the contact between material points and DEM particles. Its capability in describing the mechanics of soil-rock mixtures is thereafter proved by comparing the simulation results with pure DEM simulations of binary mixtures and laboratory tests of soil-rock mixtures. It is demonstrated that MPM-DEM can reproduce the stress–strain response of soil-rock mixtures and capture the influence of rock contents and rock sizes. In addition, a coarse-graining modelling scheme is implemented, i.e., representing the soil particles with fewer material points, which significantly increases the efficiency compared with pure DEM. Our proposed method provides a novel way to model soil-rock mixtures with reasonable computational efforts, which sheds light on simulating large-scale soil-rock mixtures in nature or engineering.

1. Introduction

Soil-rock mixtures are abundant in geotechnical engineering and have complex physical and mechanical characteristics such as heterogeneity and nonlinearity. (Hu et al., 2018). The complexity of the soil-rock mixture is mainly due to the difference in size and physical properties between its two components, i.e., soil and rock (Xu and Zhang, 2021). Accurately reproducing and predicting the behaviour of soil-rock mixtures is a difficult scientific problem and is also of great importance in the early warning and protection of natural disasters, such as debris flows and landslides (Iverson, 1997; Schuster and Highland, 2007).

Due to the presence of the large-size rock blocks and small-size soil particles that make up the unique meso-structural characteristics of the soil-rock mixture, it poses a huge threat to numerical modelling. In particular, when the particle size ratio between rock and soil is large, the heterogeneity and nonlinearity caused by the mechanical behaviours from different scales are enlarged, causing the description to diverge from reality. Generally, three kinds of methods, i.e., continuous, discrete and hybrid modelling schemes, can be used to study soil-rock mixture problems (Ren et al., 2022).

In continuum mechanics methods, such as the finite element method (FEM) (Ye et al., 2005; Yang et al., 2012; Cen et al., 2020), finite difference method (FDM) (Li and Chu, 2019; Gao et al., 2020; Nasiri and Hajiazizi, 2020), finite volume method (FVM) (Valiani et al., 2002; Serrano-Pacheco et al., 2009) and meshfree methods (Dong and Grabe, 2018; Navas et al., 2018; Wang et al., 2020; Li et al., 2022), the soil-rock mixture is normally assumed to be a continuous medium. The mechanical behaviour of the soil-rock mixture is normally described with a phenomenological macro constitutive model, while the micro mechanism cannot be modelled. In some cases, soil-rock mixtures are treated as homogeneous materials in continuous methods to reduce the complexity of the numerical models, where the rocks and soils are distinguished easily by assigning different properties (Xu et al., 2008; Zhao et al., 2021). Meanwhile, the random field theory (Zhu and Zhang, 2013; Dyson and Tolooiyan, 2019a) is also introduced in some research to consider the heterogeneity of soil-rock mixture behaviour, such as the random finite element method (RFEM) (Huang et al., 2010; Dyson and Tolooiyan, 2019b) and the random material point method (RMPM)

* Corresponding authors.
E-mail addresses: bwang@whrsm.ac.cn (B. Wang), dwang@mail.whrsm.ac.cn (D. Wang).

https://doi.org/10.1016/j.compgeo.2023.105508
Received 16 January 2023; Received in revised form 7 April 2023; Accepted 28 April 2023
Available online 10 May 2023

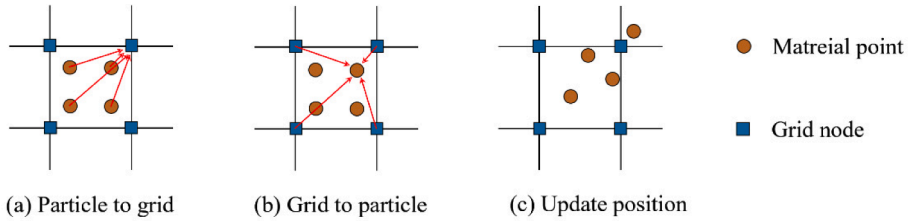

Fig. 1. Standard MPM process.

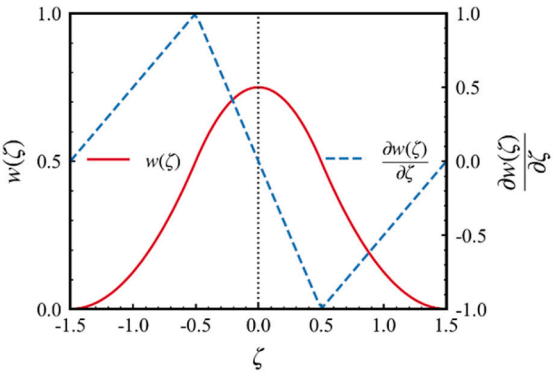

Fig. 2. 2-order B-spline basis function and its derivative.

(Remmerswaal et al., 2021). However, in this scheme, the interface between soil and rock is considered inseparable, and it overestimates the cohesion and friction between soil and rock. In summary, the simplifications in continuum mechanics methods make it an efficient approach to solving soil-rock mixture problems, but the microscopic interaction between soil and rock is neglected, making it difficult to describe and capture the micro mechanisms of soil-rock mixtures in detail.

In terms of discrete methods such as the DEM (Xu et al., 2016; Ji et al., 2022; Yao et al., 2022), soil and rock are modelled as individual particles (or blocks). There is no doubt that the microscopic interaction between particles of different grain sizes can be described in detail using discrete methods. However, when the particle size ratio between the rock and soil is large, the number of soil particles can be extremely large, which makes simulations impractical. On the other hand, if the particle size is too small, the time interval must be reduced to be very small to ensure stability, thereby making the simulation very time-consuming. Therefore, to ensure the accuracy and efficiency of the DEM in terms of simulating soil-rock mixtures, a reference particle size needs to be preset. However, it is normally much larger than the physical size of soil particles, thereby making the simulations diverge from reality. Furthermore, the parameters of a single soil particle, which may influence the mechanical behaviour of the soil-rock mixture, are usually difficult to determine through physical experiments.

Hybrid methods, such as smooth particle hydrodynamics and discrete element method coupling scheme (SPH-DEM) and MPM-DEM, have also been developed in recent years. To our knowledge, MPM-DEM coupling scheme is mainly developed in two directions. Firstly, MPM-DEM hierarchical multi-scale simulations, where a bunch of DEM particles are incorporated to represent a MPM particle, in order to connect the micro and macro soil behaviors (Wang et al., 2022; Wang et al., 2023). More specifically, the microscopic mechanism at the grain level can be obtained by the DEM, and the macroscopic mechanical behaviour can be obtained by continuous methods such as SPH and MPM. Secondly, MPM-DEM mixed simulations (Liu et al., 2018; Yue et al., 2018; Chen et al., 2021; Jiang et al., 2022; Ren et al., 2022, Singer et al., 2022), where DEM particles and MPM particles are basically placed in a unified framework, but representing different materials, which may differ in particle sizes or properties, e.g., rocks and soils. Some simulations of debris flows have been attempted using the SPH-DEM method (Trujillo-Vela et al., 2020; Luo et al., 2022). However, in the existing simulations, the DEM is only used to simulate some boulders scattered in the SPH debris slurry. In view of the small number of boulders, the debris slurry and boulders are still two individual parts rather than a mixture, and the gradation characteristics existing in the debris flow are ignored.

Therefore, we propose a coupled MPM-DEM method to simulate soil-rock mixtures in which soils are treated with continuum methods and rocks are modelled by the DEM. As for the novelty of the paper, we would like to emphasize its successful applications in modelling soil-rock mixtures with gradation characteristics. Due to the utilization of the contact force coupling scheme, material points will be converted to DEM particles with a ghost radius in the scheme, so that the contact force between the DEM particles and material points can be calculated based on DEM contact models. Meanwhile, since the ghost radius is given to each material point, the gradation characteristics of the mixture can then be reflected. As compared to the pure DEM simulations, due to the applications of MPM (continuum method) for modelling the numerous fine (soil) particles, the computational efficiency can thereby be greatly improved. Moreover, like the coarse-graining modelling scheme utilized in DEM, we applied the coarse-graining modelling scheme to the MPM part in this method, where a few small MPM particles are replaced by a large MPM particle, aiming to model soil-rock mixtures with extremely large particle size ratios, and further reducing computational resource requirements. Finally, GPU-accelerated MPM code based on the compute unified device architecture (CUDA) is developed to enhance its efficiency and tackle the computational cost associated with numerous material points' mechanical behaviours. Note that, the DEM part in our current MPM-DEM simulation is developed based on CPU without accelerating strategies, and it is expected that a GPU-accelerated DEM will be carried out in the near future, thereby making a unified GPU-accelerated environment for the whole simulation, and leading to a more realistic and large-scale problem description finally.

The whole paper is organized as follows: The basic theories of the MPM and DEM are provided first in Section 2.1, and the key idea, formulations and implementation procedures of the MPM-DEM are illustrated in Sections 2.2-2.4. Then, two simple examples, namely, ball impacting and block sliding, are introduced to illustrate the accuracy of the normal and tangential contact models, respectively, in Section 3. Afterwards, a comparative study between the MPM-DEM and DEM is provided in Section 4.1, demonstrating the effectiveness of the MPM-DEM in terms of simulating granular materials with gradations via a series of triaxial tests of binary granular mixtures. Thereafter, a coarse-graining modelling scheme based on the operation of replacing a set of small particles with one larger material point is proposed in Section 4.2 and validated using triaxial models simplified from DEM samples with a particle size ratio of 1:10. Finally, a set of laboratory medium-sized triaxial tests are simulated using the proposed coarse-graining modelling scheme to demonstrate its capacity to solve soil-rock mixture problems in Section 5. In Sections 6 and 7, some discussions and conclusions about the proposed MPM-DEM method are provided.

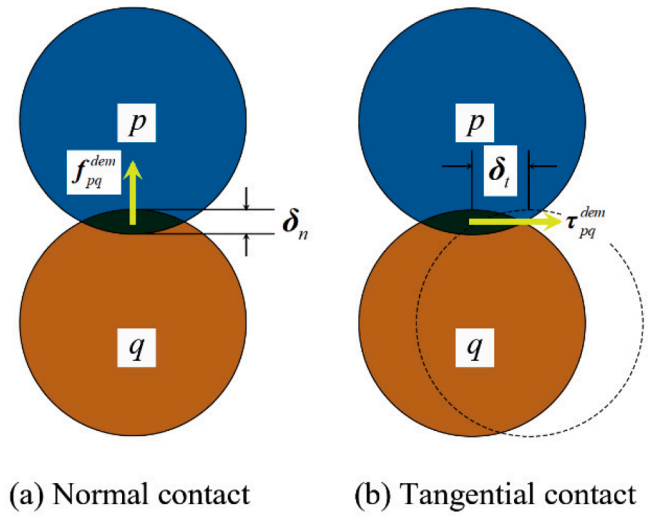

Fig. 3. Normal and tangential force calculation scheme.

2. Construction of the coupled MPM-DEM method

To improve the readability of the paper, the MPM and DEM theories are introduced first in this section. Some variables shared by the MPM and DEM are distinguished by the superscripts *mpm* and *dem*.

2.1. Basic theory of the MPM and DEM

2.1.1. Formulation of the MPM

In continuum mechanics, mass conservation and momentum conservation can be written as two partial differential equations (PDEs) as follows:

Mass conservation:

$$\dot{\rho} + \rho \nabla \cdot \dot{\boldsymbol{u}} = 0 \tag{1}$$

Momentum conservation:

$$\rho \ddot{\boldsymbol{u}} = \nabla \cdot \boldsymbol{\sigma} + \boldsymbol{f}_b \tag{2}$$

where ρ is the density of the material, $\dot{\rho}$ is the change rate of density with time, $\dot{\boldsymbol{u}}$ is the velocity, $\ddot{\boldsymbol{u}}$ is the acceleration, $\boldsymbol{\sigma}$ is the stress and $\boldsymbol{f}_b$ is the body force.

For mass conservation, a simple treatment in the MPM is to give a mass that does not change with time to each material point, so it is not detailed here. In terms of momentum conservation, the equation can be transformed into a weak form, as shown in Eq. (3) using the Galerkin method as follows:

$$\int_\Omega \delta \boldsymbol{u} : \boldsymbol{\sigma} \mathrm{d}\Omega + \int_\Omega \delta \mathbf{u} \cdot \mathbf{f}_b \mathrm{d}\Omega + \int_\Gamma \delta \mathbf{u} \cdot \mathbf{f}_\Gamma \mathrm{d}\Gamma = \int_\Omega \delta \mathbf{u} \cdot \rho \ddot{\mathbf{u}} \mathrm{d}\Omega \tag{3}$$

where $\delta \boldsymbol{u}$ is the visual displacement, Ω is the problem domain, Γ is the boundary of the problem domain, $\boldsymbol{f}_b$ refers to the body force and $\boldsymbol{f}_\Gamma$ is the surface traction acting on the boundaries.

To calculate the integrations in Eq. (3) using MPM, a background mesh is needed, as shown in Fig. 1. Generally, three basic steps can be summarized in the standard MPM. First, the information on the material points is mapped to the grid nodes to form the discrete momentum conservation equations. Second, the equations on the grid nodes are solved, and the information is mapped back from the grid nodes to the material points. Finally, variables, such as the positions and velocities of the material points, are updated. Some details may be different due to the stress and velocity updating scheme. In this work, the MUSL stress updating scheme (Kan et al., 2021) and FLIP velocity updating scheme (Brackbill and Ruppel, 1986; Brackbill et al., 1988) are adopted; see Section 2.4 for details. The discrete form of the momentum conservation equation can be written as Eq. (4), which is established following a similar process as that of the standard FEM (Zhang et al., 2001):

$$\boldsymbol{F}_{ext} + \boldsymbol{F}_{int} = \boldsymbol{M}\ddot{\boldsymbol{U}} \tag{4}$$

where $\boldsymbol{F}_{ext}$ and $\boldsymbol{F}_{int}$ are the global external force vector and internal force vector, respectively, $\boldsymbol{M}$ is the mass matrix and $\ddot{\boldsymbol{U}}$ is the global acceleration vector. If a lumped mass matrix (Wu, 2006) is used, Eq. (4) can be solved on each grid node individually, which is shown in Eq. (5) as follows:

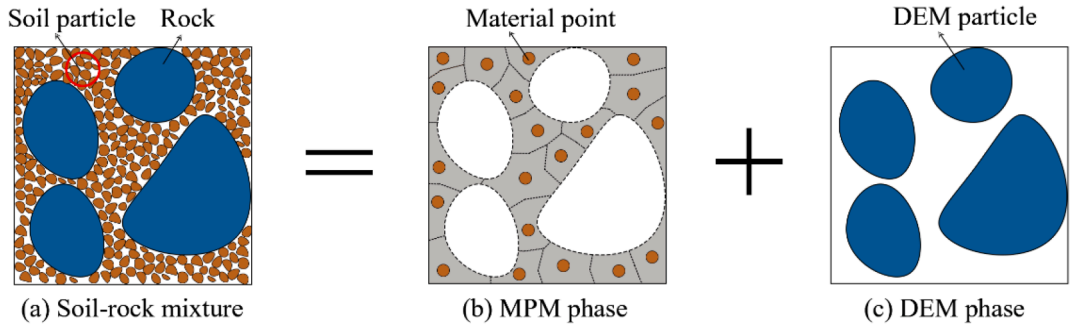

Fig. 4. MPM-DEM treatment for soil-rock mixtures.

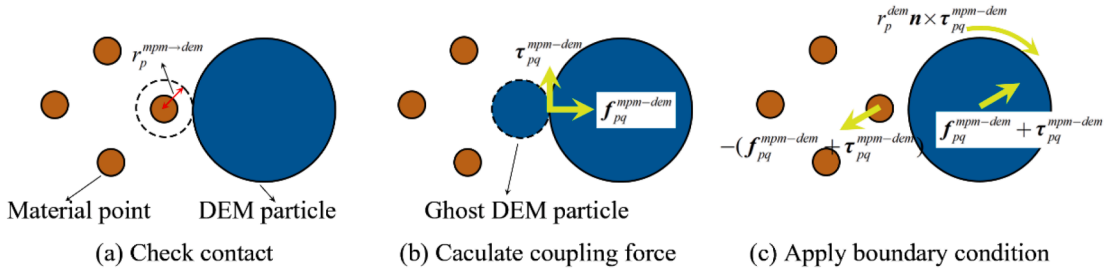

Fig. 5. Contact force coupling scheme.

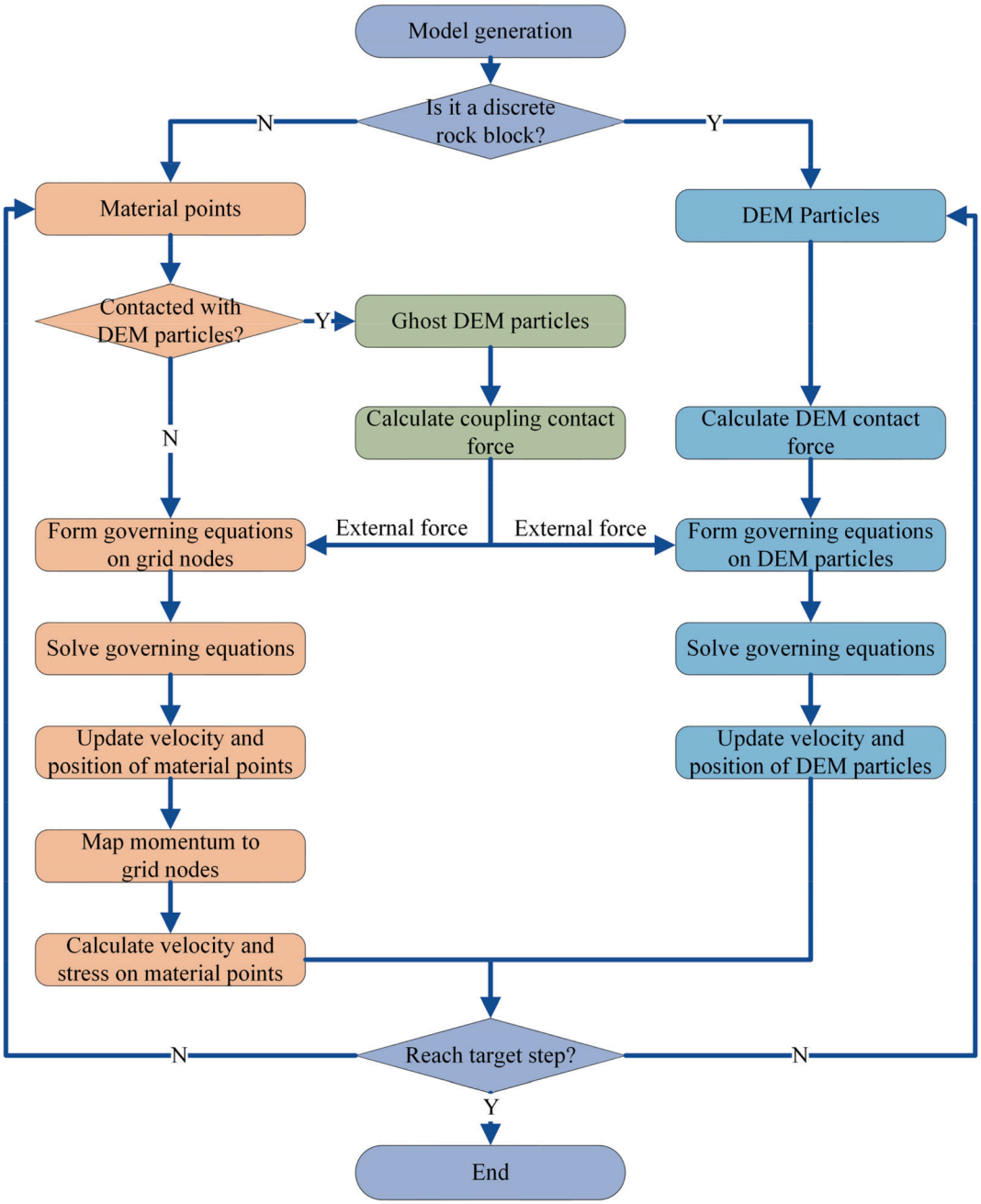

Fig. 6. Implementation procedure of the coupled MPM-DEM.

$$\boldsymbol{f}_{I,ext}+\boldsymbol{f}_{I,int}=m_I\ddot{\boldsymbol{u}}_I \tag{5}$$

where $\boldsymbol{f}_{I,ext}$ and $\boldsymbol{f}_{I,int}$ are the external and internal forces on grid node I, respectively, and m_I and $\ddot{\boldsymbol{u}}_I$ refer to the mass and acceleration of grid node I, respectively. $\boldsymbol{f}_{I,int}$ and $\boldsymbol{f}_{I,ext}$ can be calculated by Eqs. (6)–(7) using a particle-to-grid scheme by introducing the shape functions, which are defined as follows:

$$\boldsymbol{f}_{I,int}=-\sum_{p,p\in gNeighbor}\boldsymbol{\sigma}_p\cdot\boldsymbol{B}_{Ip}V_p^{mpm} \tag{6}$$

$$\boldsymbol{f}_{I,ext}=\sum_{p,p\in gNeighbor}\boldsymbol{f}_p^{mpm}N_{Ip}+\boldsymbol{f}_{I,\Gamma} \tag{7}$$

Similarly, the nodal mass and nodal velocity can also be calculated in this way and are expressed as follows:

$$m_I=\sum_{p,p\in gNeighbor}m_p^{mpm}N_{Ip} \tag{8}$$

$$\dot{\boldsymbol{u}}_I=\frac{1}{m_I}\cdot\sum_{p,p\in gNeighbor}m_p^{mpm}\dot{\boldsymbol{u}}_p^{mpm}N_{Ip} \tag{9}$$

where $\boldsymbol{\sigma}_p$, V_p^{mpm}, $\boldsymbol{f}_p^{mpm}$, m_p^{mpm} and $\dot{\boldsymbol{u}}_p^{mpm}$ are the stress, volume, body force, mass and velocity on material point p, respectively, and $\boldsymbol{f}_{I,\Gamma}$ is the surface traction applied on grid node I calculated by surface integration. N and $\boldsymbol{B}$ are the weighting function and the vector of its spatial partial derivative, and *gNeighbor* represents the neighbour particle list of the concerned grid node. A 2-order B-spline (Gan et al., 2018) basis function (as shown in Fig. 2) is used in this paper to form the weighting functions to reduce the cell-crossing error (Yamaguchi et al., 2021) and is defined in Eq. (10) as follows:

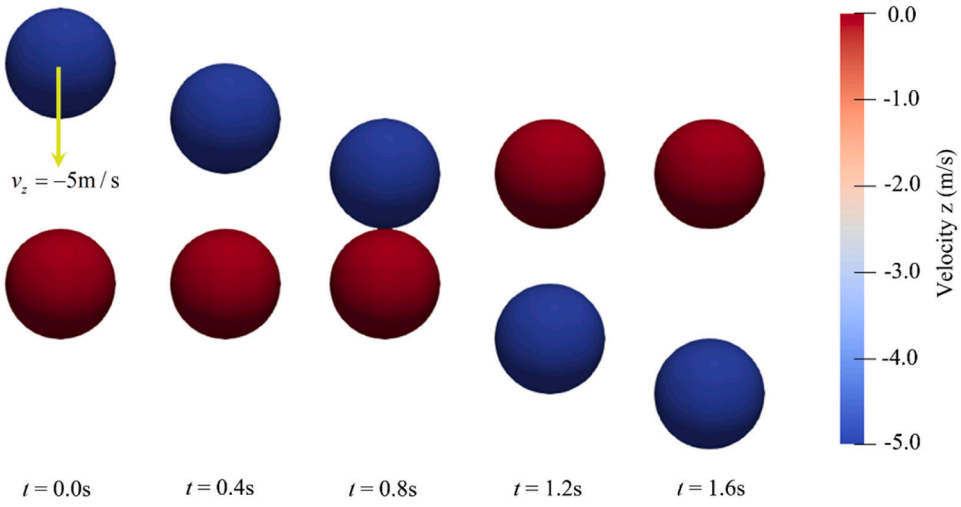

(a) Impact between single DEM particle and single MPM particle

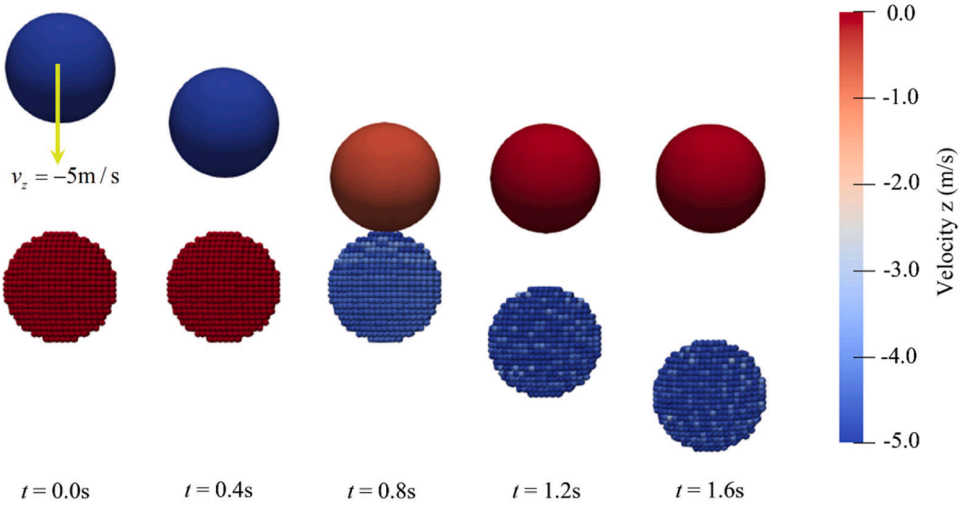

(b) Impact between single DEM particle and Multiple MPM particles

Fig. 7. Momentum exchange process in ball impacting example.

Table 1
The parameters and the initial settings of the ball impacting example.

Parameters and initial settings	Single DEM - Single MPM		Single DEM - Multiple MPM	
	DEM ball	MPM ball	DEM ball	MPM ball
Total mass (kg)	0.3351			
Young's modulus (GPa)	1.0			
Poisson's ratio	0.2			
Friction coefficient	0.8			
Time interval (s)	1.0e-6			
Total time (s)	1.6			
Initial velocity (m/s)	−5.0	0.0	−5.0	0.0
Particle number	1	1	1	4224

$$w(\zeta) = \begin{cases} 0.75 - |\zeta|^2 & 0 \leqslant |\zeta| < 0.5 \\ 0.5 \cdot (1.5 - |\zeta|)^2 & 0.5 \leqslant |\zeta| < 1.5 \\ 0 & 1.5 \leqslant |\zeta| \end{cases} \tag{10}$$

where ζ is the local coordinate of a material point, and the weighting function can be formed by the B-spline basis functions $w(\zeta)$ as follows:

$$N = w(\zeta_x) \cdot w(\zeta_y) \cdot w(\zeta_z) \tag{11}$$

$$\boldsymbol{B} = \begin{bmatrix} \dfrac{\partial w(\zeta_x)}{\partial x} \cdot w(\zeta_y) \cdot w(\zeta_z) \\ w(\zeta_x) \cdot \dfrac{\partial w(\zeta_y)}{\partial y} \cdot w(\zeta_z) \\ w(\zeta_x) \cdot w(\zeta_y) \cdot \dfrac{\partial w(\zeta_z)}{\partial z} \end{bmatrix} \tag{12}$$

where ζ_x, ζ_y and ζ_z are the local coordinates of the material point in three directions.

2.1.2. Formulation of the DEM

In the DEM, for each particle, mass conservation is clearly satisfied because its mass is a constant. The momentum conservation can be expressed as shown in Eqs. (13)–(14), which are expressed as follows:

$$\boldsymbol{f}_p^{dem} + \boldsymbol{\tau}_p^{dem} + \boldsymbol{f}_p^{dem,b} = m_p^{dem} \ddot{\boldsymbol{u}}_p^{dem} \tag{13}$$

$$\boldsymbol{T}_p^{dem} + \boldsymbol{T}_p^{rolling} = \boldsymbol{I}_p \ddot{\boldsymbol{\theta}}_p^{dem} \tag{14}$$

$$\boldsymbol{T}_p^{dem} = \sum_{q,q \in pContact} \left(r_p^{dem} - \frac{\|\boldsymbol{\delta}_n\|}{2} \right) \boldsymbol{n} \times \boldsymbol{\tau}_p^{dem} \tag{15}$$

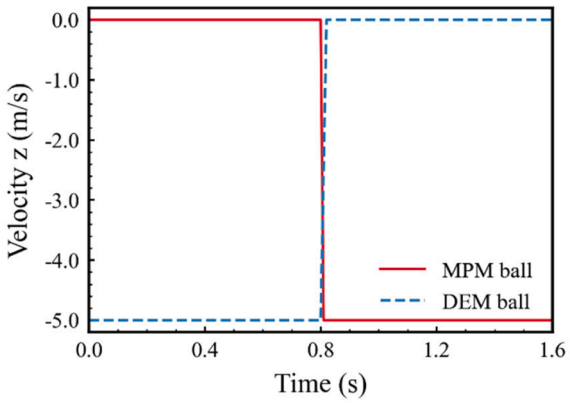

(a) Velocity of single DEM – single MPM

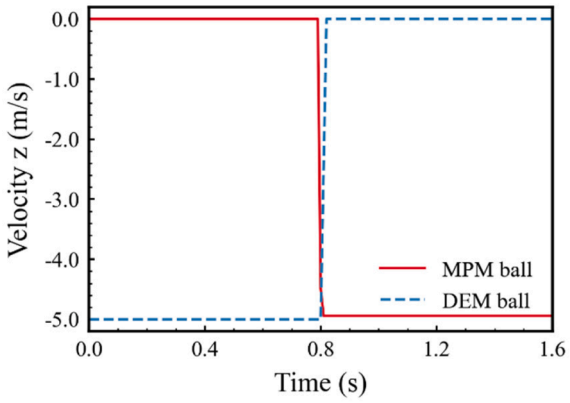

(b) Velocity of single DEM – multiple MPMs

Fig. 8. Velocities of two ball impacting cases with time.

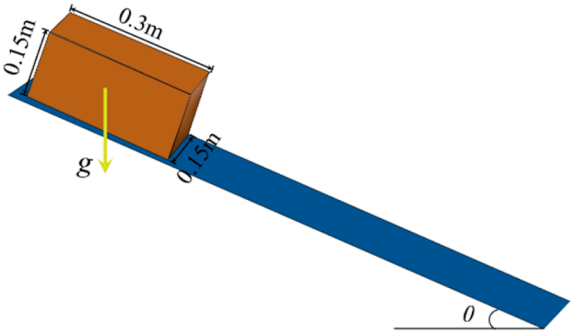

Fig. 9. Schematic diagram of the block sliding example.

where f_p^{dem}, m_p^{dem} and $\ddot{\boldsymbol{u}}_p^{dem}$ are the normal contact force, mass and acceleration of the DEM particle p, $\boldsymbol{\tau}_p^{dem}$ is the tangential contact force, $f_p^{dem,b}$ is the body force, e.g., gravity, $\boldsymbol{n}$ is the unit normal vector, $\boldsymbol{T}_p^{dem}$ is torque from other DEM particles, $\boldsymbol{T}_p^{rolling}$ is the torque caused by rolling friction, r_p^{dem} is the radius of particle p, $\boldsymbol{\delta}_n$ is the normal overlap between two contacted particles, and $\boldsymbol{I}_p$ and $\ddot{\boldsymbol{\theta}}_p$ are the moment of inertia and the angular acceleration of particle p, respectively. The contributions from all contacted particles should be considered in the calculation of f_p^{dem} and $\boldsymbol{\tau}_p^{dem}$, which are as follows:

$$\boldsymbol{f}_p^{dem} = \sum_{q,q\in pContact} \boldsymbol{f}_{pq}^{dem} \tag{16}$$

$$\boldsymbol{\tau}_p^{dem} = \sum_{q,q\in pContact} \boldsymbol{\tau}_{pq}^{dem} \tag{17}$$

where $\boldsymbol{f}_{pq}^{dem}$ and $\boldsymbol{\tau}_{pq}^{dem}$ are the contact forces between particles p and q in the normal and tangential directions, respectively, and they can be calculated using the Hertz-Mindlin contact theory (Goniva et al., 2012). *pContact* denotes the contacted particle list of the concerned particle p. As shown in Fig. 3, the normal contact force is solved based on the normal overlap between the two particles, and the tangential force is calculated by the relative tangential displacement of the contact point and Coulomb's friction law.

$$\boldsymbol{f}_{pq}^{dem} = -k_n\boldsymbol{\delta}_n - \eta_p^{nor}\dot{\boldsymbol{u}}_{pq}^{nor,dem} \tag{18}$$

$$\boldsymbol{\tau}_{pq}^{dem} = \begin{cases} -\int_{t_{c,0}}^{t} k_t\dot{\boldsymbol{u}}_{pq}^{tan,dem}dt - \eta_p^{tan}\dot{\boldsymbol{u}}_{pq}^{tan,dem}, \left\|\boldsymbol{\tau}_{\mathrm{pq}}^{\mathrm{dem}}\right\| \leqslant \mu\left\|\mathbf{f}_{\mathrm{pq}}^{\mathrm{dem}}\right\| \\ -\mu\left\|\boldsymbol{f}_{pq}^{dem}\right\|\boldsymbol{t}, \left\|\boldsymbol{\tau}_{pq}^{dem}\right\| > \mu\left\|\boldsymbol{f}_{pq}^{dem}\right\| \end{cases} \tag{19}$$

where k_n and k_t are elastic constants in the normal and tangential directions, respectively, and they can be calculated following Eqs. (20)–(21). η_p^{nor} and η_p^{tan} are the normal and tangential viscoelastic damping constants, $\boldsymbol{t}$ is the tangential unit vector and μ is the friction coefficient. $\dot{\boldsymbol{u}}_{pq}^{nor,dem}$ and $\dot{\boldsymbol{u}}_{pq}^{tan,dem}$ are normal and tangential relative velocities, respectively.

$$k_n = \frac{4}{3}\|\boldsymbol{\delta}_n\|^{\frac{1}{2}}\left(\frac{1-\left(v_p^{dem}\right)^2}{E_p} + \frac{1-\left(v_q^{dem}\right)^2}{E_q}\right)^{-1} \cdot \left(\frac{r_p^{dem}+r_q^{dem}}{r_p^{dem}\cdot r_q^{dem}}\right)^{-1/2} \tag{20}$$

$$k_t = 4\|\boldsymbol{\delta}_n\|^{\frac{1}{2}}\left(\frac{\left(2-v_p^{dem}\right)\cdot\left(1+v_p^{dem}\right)}{E_p} + \frac{\left(2-v_q^{dem}\right)\cdot\left(1+v_q^{dem}\right)}{E_q}\right)^{-1} \cdot \left(\frac{r_p^{dem}+r_q^{dem}}{r_p^{dem}\cdot r_q^{dem}}\right)^{-1/2} \tag{21}$$

where v_p^{dem} and v_q^{dem} are Poisson's ratios of particles p and q, respectively, E_p and E_q are Young's moduli, and r_p^{dem} and r_q^{dem} represent the radii.

2.2. MPM-DEM scheme for soil-rock mixtures

According to the characteristics of soil and rock, continuous and discontinuous methods can be used to model soil and rock, respectively. The soil mass is composed of many soil particles and exhibits the characteristics of a continuous medium. It is difficult to obtain the properties of a single soil particle using laboratory tests, but it is easy to obtain its macroscopic mechanical response to describe its mechanical behaviour through a constitutive model using continuous methods. Rocks are scattered in the soil mass, which usually has higher strength compared with the soil mass. They are distinct from soil and other rocks, which can be described with discrete methods.

As shown in Fig. 4, the MPM and DEM are used to construct this hybrid continuous-discrete scheme to model soil-rock mixtures. The soil mass is treated as a continuous medium and discretized into a series of material points, of which the mechanical properties can be described with a constitutive model. The rocks are modelled with DEM particles for simplicity. Various shapes of DEM particles (Zhao and Zhao, 2019) make it possible to model rocks with almost any shape, and the convenient contact theory makes it suitable for describing the interaction between multiple rocks. If the strength of rocks is very high and only small deformation occurs during the whole physical process, a rock can

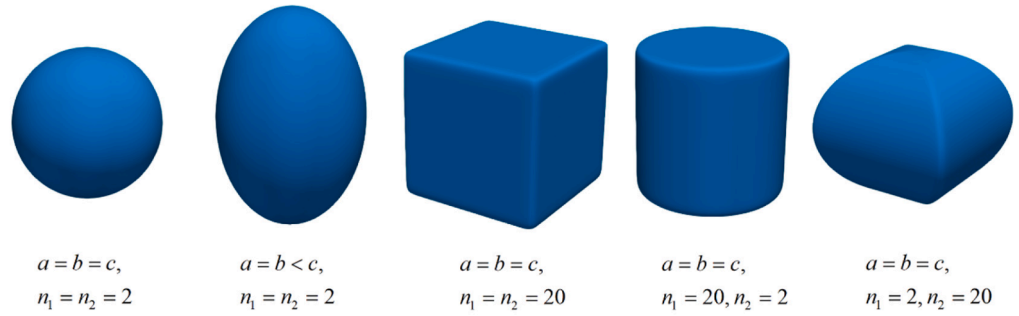

Fig. 10. Superquadric particles with different parameters.

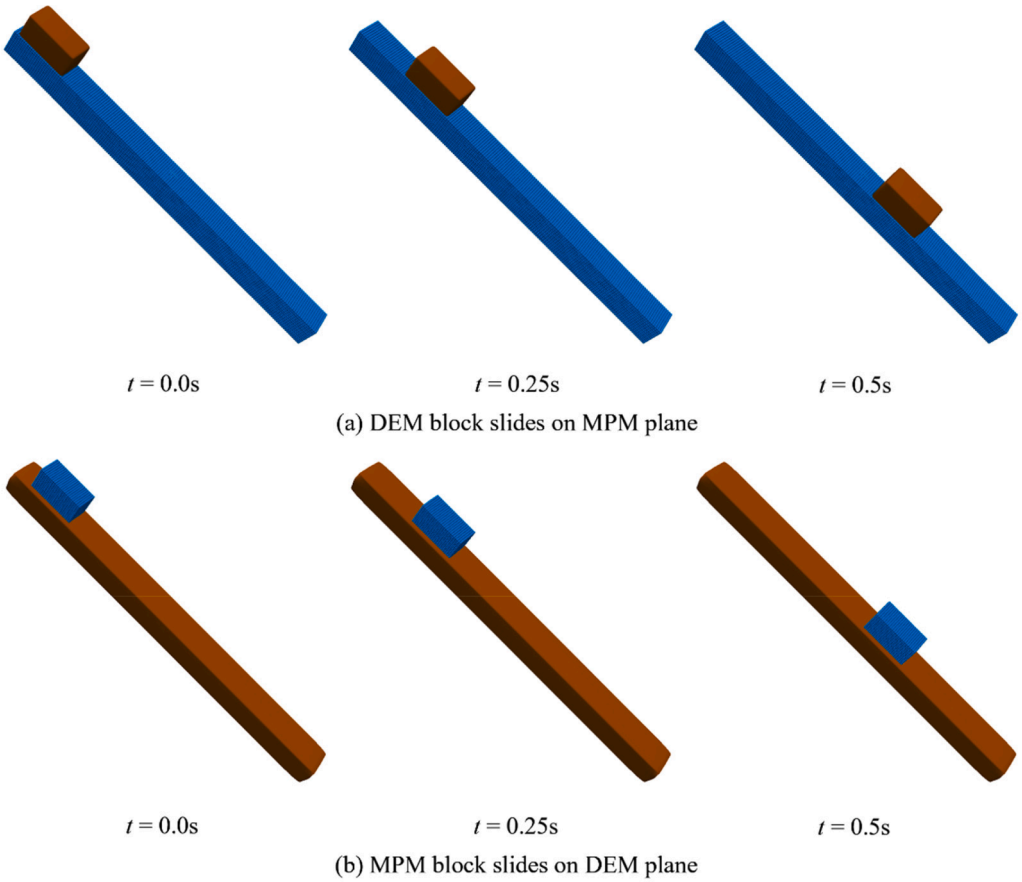

Fig. 11. Position of the block on the plane at different times.

be modelled with only one DEM particle, while if the rock is broken, it can be modelled with multiple DEM particles with the particle breakage theory (Zhou et al., 2020; Wang et al., 2021; Ni et al., 2022). For simplicity, spherical DEM particles are used in the simulations of this paper, and particle breakage is not considered.

The interactions between rock and soil, including the frictional and cohesive characteristics, can be described by the contact between these two components. In our MPM-DEM scheme, various contact models approved in the DEM can be used to calculate the contact force between rock and soil. However, a material point cannot directly interact with DEM particles, and a scheme converting material points in contact with DEM particles into ghost DEM particles is proposed; see Section 2.3 for details.

2.3. Formulation of the MPM-DEM

The coupling of the two methods is based on the laws of mass conservation and momentum conservation. The mass conservation is automatically satisfied because the model can be simplified to a series of particles with constant masses in both the MPM and DEM. Based on momentum conservation, the contact force is used to link the two methods (see Fig. 5). Because the contact force is a pair of forces with equal magnitude and opposite directions and the force transmission process is also accompanied by momentum transmission, the contact force coupling scheme thereby automatically meets the momentum conservation.

As shown in Fig. 5, the key idea of the contact force coupling scheme is to treat the material points in contact with DEM particles as ghost DEM particles to calculate the coupling contact force and then apply the

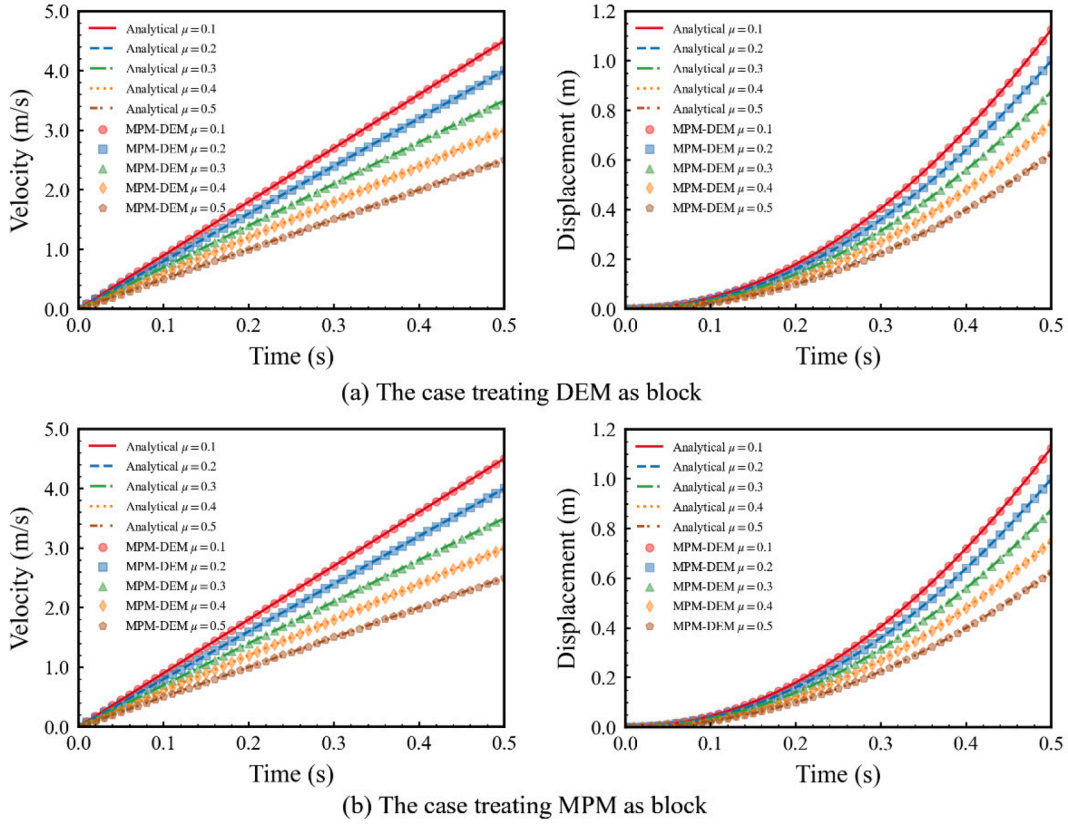

Fig. 12. Velocities and displacements of the block with time.

coupling contact force as an external force to the DEM and MPM. It can be summarized into three basic steps. First, a ghost radius $r_p^{mpm\to dem}$ is introduced to check whether a material point is in contact with any DEM particles. Thereafter, the contacted material points are converted into ghost DEM particles, and the coupling contact force is calculated using the Hertz-Mindlin contact theory. Finally, the ghost DEM particles are converted back to material points, the coupling contact force is applied to the MPM and DEM parts, and the two parts then enter their own calculation process. It is worth noting that the material points that are not in contact with the DEM particles do not participate in the coupling process, leading to very low computational effort.

For convenience, the ghost radius can be directly calculated from the volume of the source material point by Ren et al. (Ren et al., 2022), while a different scheme that introduces the porosity is used in this work. The radius of a ghost DEM particle can be calculated as shown in Eq. (22), which is expressed as follows:

$$r_p^{mpm\to dem} = \sqrt[3]{\frac{3}{4\pi}\cdot V_p^{mpm}\cdot\left(1-\kappa_p\right)} \tag{22}$$

where κ_p is the porosity of material point p. This scheme allows the MPM-DEM model to be directly constructed by classical DEM modelling schemes, such as the volume expansion method. This ensures that there is a reasonable degree of initial overlap, without introducing contact gaps, and helps to establish the model under a correct initial stress state.

The total normal and tangential coupling contact force acting on the DEM particle and the contacted material points can be calculated as shown in Eqs. (23)–(24), which are expressed as follows:

$$\boldsymbol{f}_p^{mpm-dem} = \sum_{q,q\in pContact} \boldsymbol{f}_{pq}^{mpm-dem} \tag{23}$$

$$\boldsymbol{\tau}_p^{mpm-dem} = \sum_{q,q\in pContact} \boldsymbol{\tau}_{pq}^{mpm-dem} \tag{24}$$

where $\boldsymbol{f}_{pq}^{mpm-dem}$ and $\boldsymbol{\tau}_{pq}^{mpm-dem}$ are the normal and tangential coupling contact forces on DEM particle p from material point q, respectively, which can be calculated by Eq. (18) and (19).

By applying $\boldsymbol{f}_p^{mpm-dem}$ and $\boldsymbol{\tau}_p^{mpm-dem}$ as external forces to DEM particle p, the coupling form of the momentum conservation equation of the DEM can be obtained as follows:

$$\boldsymbol{f}_p^{dem} + \boldsymbol{\tau}_p^{dem} + \boldsymbol{f}_p^{mpm-dem} + \boldsymbol{\tau}_p^{mpm-dem} + \boldsymbol{f}_p^{dem,b} = m_p^{dem}\ddot{\boldsymbol{u}}_p^{dem} \tag{25}$$

$$\boldsymbol{T}_p^{dem} + \boldsymbol{T}_p^{mpm-dem} + \boldsymbol{T}_p^{rolling} = \boldsymbol{I}_p\ddot{\boldsymbol{\theta}}_p^{dem} \tag{26}$$

$$\boldsymbol{T}_p^{mpm-dem} = \sum_{q,q\in pContact}\left(r_p^{mpm\to dem} - \frac{\|\boldsymbol{\delta}_n\|}{2}\right)\boldsymbol{n}\times\boldsymbol{\tau}_p^{mpm-dem} \tag{27}$$

where $\boldsymbol{T}_p^{mpm-dem}$ is the torque caused by the material points in contact with the current particle. A similar treatment can be applied to the MPM momentum conservation equation, so a new governing equation of the MPM can be obtained as follows:

$$\bar{\boldsymbol{f}}_{I,ext} + \boldsymbol{f}_{I,int} = m_I\ddot{\boldsymbol{u}}_I \tag{28}$$

where $\bar{\boldsymbol{f}}_{I,ext}$ can be calculated as follows:

$$\bar{\boldsymbol{f}}_{I,ext} = \sum_{p,p\in gNeighbor}\left(\boldsymbol{f}_p^{mpm} - \boldsymbol{f}_p^{mpm-dem} - \boldsymbol{\tau}_p^{mpm-dem}\right)\cdot N_{Ip} + \boldsymbol{f}_{I,\Gamma} \tag{29}$$

Note that the contact coupling scheme only changes the external force boundary conditions of the MPM and DEM, and the introduction of ghost DEM particles does not affect their own solution process, which means that the governing equations can be solved concurrently. This process will be illustrated in detail in Section 2.4.

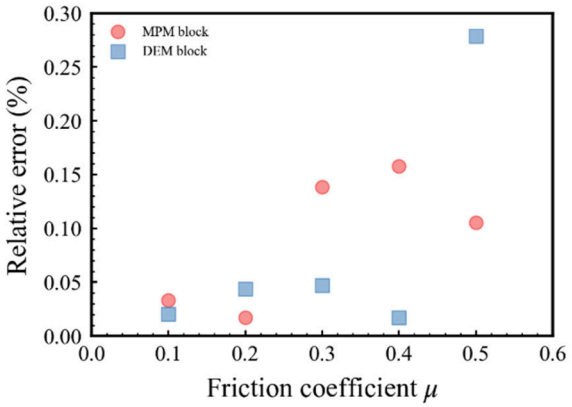

(a) Relative error of velocity

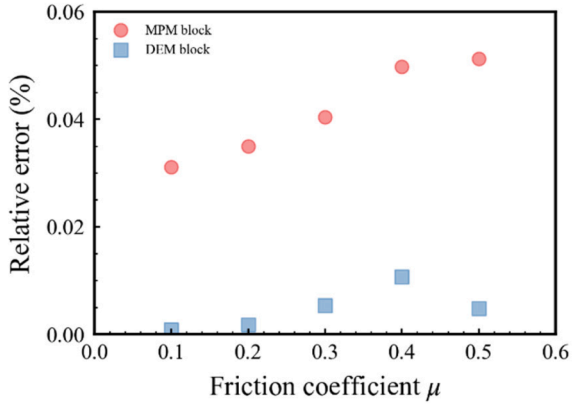

(b) Relative error of displacement

Fig. 13. Relative error of the maximum velocity and displacement.

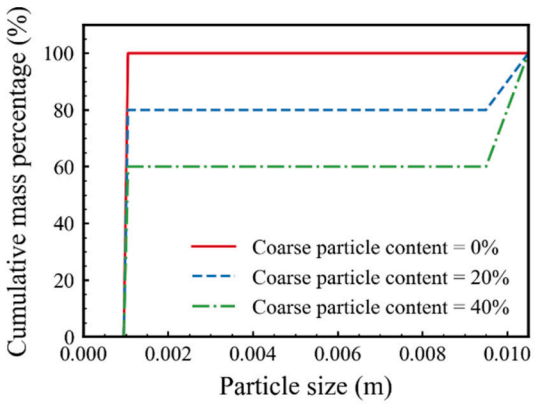

Fig. 14. Grading curves of binary granular mixture triaxial samples.

2.4. Implementation procedure of the coupled MPM-DEM

To solve the coupling governing equations of the MPM and DEM, a central difference time integration scheme (Berzins, 2022) has been introduced. The MUSL stress update scheme and FLIP velocity update scheme are used in this research to ensure the conservation of energy. The calculation procedure of the MPM-DEM is summarized in this section and simplified in a diagram in Fig. 6.

Table 2
The number of particles in binary granular mixtures.

Coarse particle content	Confining pressure	Number of fine particles	Number of coarse particles	Total number of particles
0%	50 kPa	512,000	0	512,000
20%	50 kPa	431,054	127	431,181
40%	50 kPa	326,236	232	326,468

The detailed implementation procedure of the coupled MPM-DEM is as follows:

(1) Preprocessing.

Establish the numerical model using a series of particles and determine their parameters. Macro-parameters can be determined through triaxial tests, while micro-parameters should be determined through some calibration simulations.

(2) Form and solve the governing equations.

Formulate the coupling governing equations using Eqs. (25)–(26) and (28), and subsequently solve the MPM nodal acceleration and DEM particle acceleration.

(3) Update the velocities and positions of particles.

a. Velocities of material point is updated using FLIP scheme:

$$\dot{\boldsymbol{u}}_p^{n+1/2,mpm} = \alpha \sum_{I,I\in\overline{pNeighbor}} N_{Ip}^n \cdot \boldsymbol{u}_I^{n+1/2} + (1-\alpha)\left(\dot{\boldsymbol{u}}_p^{n-1/2,mpm} + \Delta t \cdot \sum_{I,I\in\overline{pNeighbor}} N_{Ip}^n \cdot \ddot{\boldsymbol{u}}_I^n\right) \tag{30}$$

where $\overline{pNeighbor}$ is the neighbour grid node list of material point p, α is the PIC damping.

Velocities of DEM particles are updated directly:

$$\dot{\boldsymbol{u}}_p^{n+1/2,dem} = \dot{\boldsymbol{u}}_p^{n-1/2,dem} + \Delta t \cdot \ddot{\boldsymbol{u}}_p^{n,dem} \tag{31}$$

$$\dot{\boldsymbol{\theta}}_p^{n+1/2,dem} = \dot{\boldsymbol{\theta}}_p^{n-1/2,dem} + \Delta t \cdot \ddot{\boldsymbol{\theta}}_p^{n,dem} \tag{32}$$

b. Positions of MPM and DEM parts are updated as follow:

$$\boldsymbol{u}_p^{n+1,mpm} = \boldsymbol{u}_p^{n,mpm} + \Delta t \cdot \sum_{I,I\in\overline{pNeighbor}} N_{Ip}^n \cdot \dot{\boldsymbol{u}}_I^{n+1/2} \tag{33}$$

$$\boldsymbol{u}_p^{n+1,dem} = \boldsymbol{u}_p^{n,dem} + \Delta t \cdot \dot{\boldsymbol{u}}_p^{n+1/2,dem} \tag{34}$$

$$\boldsymbol{\theta}_p^{n+1,dem} = \boldsymbol{\theta}_p^{n,dem} + \Delta t \cdot \dot{\boldsymbol{\theta}}_p^{n+1/2,dem} \tag{35}$$

(4) Update the stress of material points.

The try stress is updated with MUSL scheme:

$$m_I^{n+1} = \sum_{p,p\in gNeighbor} N_{Ip}^{n+1} m_p^{mpm} \tag{36}$$

$$\dot{\boldsymbol{u}}_I^{n+1/2} = \frac{1}{m_I^{n+1}} \cdot \sum_{p,p\in gNeighbor} N_{Ip}^{n+1} m_p^{mpm} \dot{\boldsymbol{u}}_p^{n+1/2} \tag{37}$$

After the nodal velocity is recalculated following Eqs. (36)–(37), the strain and spinor can be determined using a grid to particle scheme. The try stress is calculated using an elastic constitutive considering the Jaumann stress rate, and then corrected to fit the Drucker-Prager yield surface.

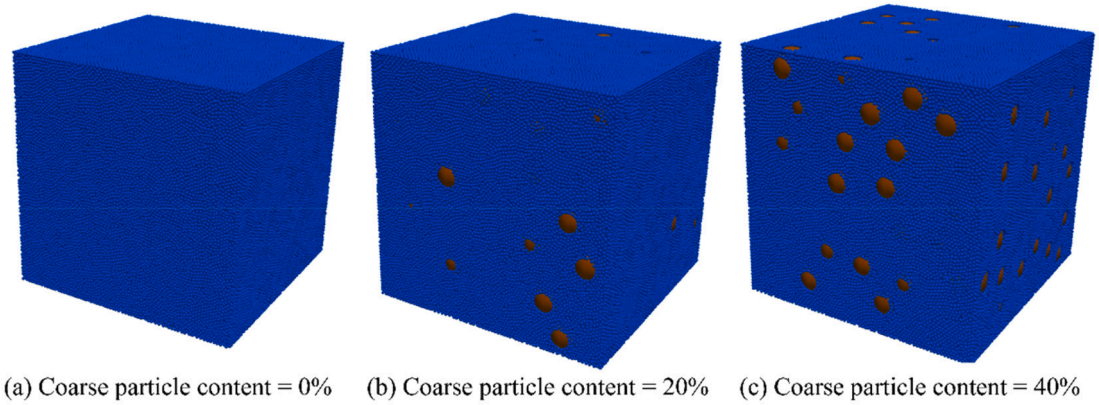

Fig. 15. Samples with a particle size ratio of 1:10 for pure DEM simulations.

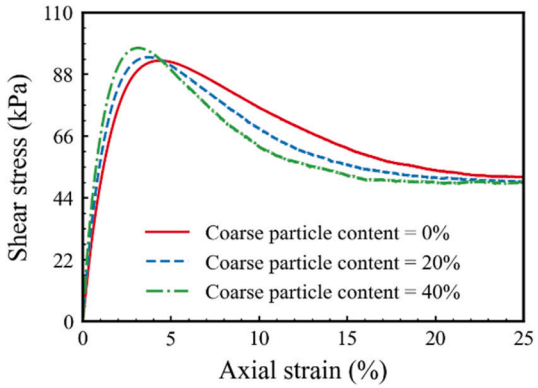

Fig. 16. Curves under different coarse particle contents.

Incidentally, to ensure the numerical stability, the Raleigh time interval is employed in this study.

$$\Delta t_{Ralrigh} = \frac{\pi r_{min}}{0.163\nu + 0.877}\sqrt{\frac{\rho}{G}} \tag{38}$$

where r_{min} minimum radius of particles, G is the shear modulus.

(5) Check if the number of steps has reached the limit.

If it reaches a critical number of steps, then end the calculation process; otherwise, go back to step (2) and continue the cycle.

3. Validation of the contact model

As stated in Sections 2.3 and 2.4, the coupling between the MPM and DEM occurs through the contact force. Therefore, two simple benchmark examples are carried out first to verify the correctness of the normal and tangential contacts.

3.1. Ball impacting for normal contact verification

The accuracy of momentum exchange between two balls is important to check the correctness of the normal contact for the MPM-DEM method. In this section, a simple ball impacting example is presented. In this example, a DEM ball moves towards an MPM ball with a constant velocity, and the momentum exchange is recorded for the whole collision process. Moreover, to make the validation more rigorous, two cases of MPM balls are considered: one is composed of a single material point (Fig. 7a), and the other involves multiple material points (Fig. 7b).

A linear-elastic constitutive model is used in the MPM part to avoid potential energy loss due to plasticity. Moreover, to show the momentum exchange between the MPM and DEM more intuitively, the masses of the MPM and DEM particles are set to be the same. The same time interval shared by the MPM and DEM, and the material properties and initial settings are provided in Table 1.

As shown in Fig. 7, in the two cases, i.e., single DEM – single MPM and single DEM – multiple MPMs, the DEM ball impacts the MPM ball after approximately 0.8 s. After the impact, the DEM ball's velocity is instantly reduced to zero, while on the contrary, the MPM ball inherits its velocity spontaneously.

The curves of the velocities with time for the MPM and DEM balls are provided in Fig. 8 using a quantitative approach. It can be clearly seen that the momentum exchange between the MPM and DEM finished in a very short time and that the momentum conservation is well satisfied. Therefore, the normal contact model between the MPM and DEM is correct and reliable.

3.2. Block sliding for tangential contact verification

For the purpose of verifying the correctness of the tangential contact model, an example of a block sliding on an inclined frictional plane is described in this section (see Fig. 9). The block has a size of 0.3 m × 0.15 m × 0.15 m. Two cases are modelled: the DEM block sliding on the MPM plane and the MPM block sliding on the DEM plane. The dip angle of the plane is 45°, and the width is 0.15 m. A series of scenarios with different friction coefficients is considered, where the friction coefficient varies from 0.1 to 0.5 at an interval of 0.1.

To simulate the block and the inclined plane using a DEM particle, the superquadric nonspherical particle is introduced, and its surface can be described using Eq. (39).

$$f(\boldsymbol{x}) = \left(\left|\frac{x}{a}\right|^{n_2} + \left|\frac{y}{b}\right|^{n_2}\right)^{n_1/n_2} + \left|\frac{z}{c}\right|^{n_1} - 1 = 0 \tag{39}$$

where x, y and z are the spatial coordinates, $\boldsymbol{x} = (x, y, z)^T$, a, b and c are the shape parameters representing the half-length of the particle along its three directions, and n_1 and n_2 are the blockiness parameters belonging to interval $[2,+\infty)$; when n_1 and n_2 are set to 2, it becomes a spherical particle. Fig. 10 demonstrates how to control its shape using the parameters in the superquadric surface equation. The shape parameters are set according to the size of the block and the plane, and the block parameters are set as $n_1 = n_2 = 20.0$ in this work.

Driven by a vertically downwards acceleration with a magnitude of $10\sqrt{2}$ m/s^2, the block slides along the plane. The Young's modulus, Poisson's ratio and density are set to be the same for both the MPM and DEM, which are 80.0 MPa, 0.3 and 2000.0 kg/m^3, respectively. The ghost radius of the material point, which is necessary for the calculation of the contact force with the DEM particles, is calculated under the assumption of a zero void ratio. The time step is chosen as 1.0e-5 s, and a total physical time of 0.5 s is simulated.

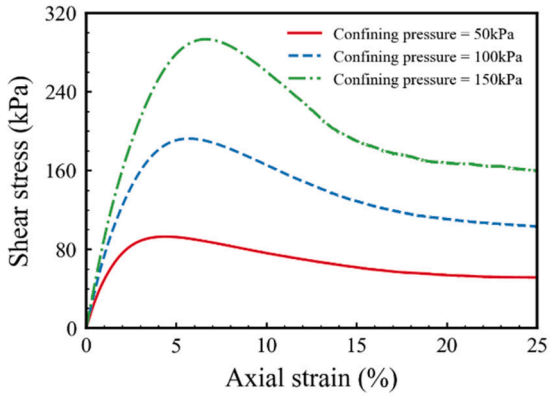

(a) Axial strain – shear stress curves

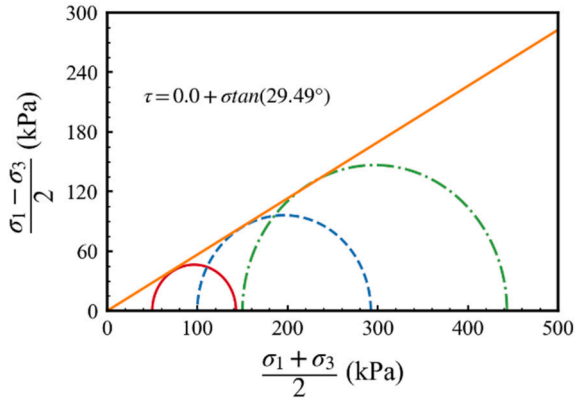

(b) Mohr stress circle of peak strength

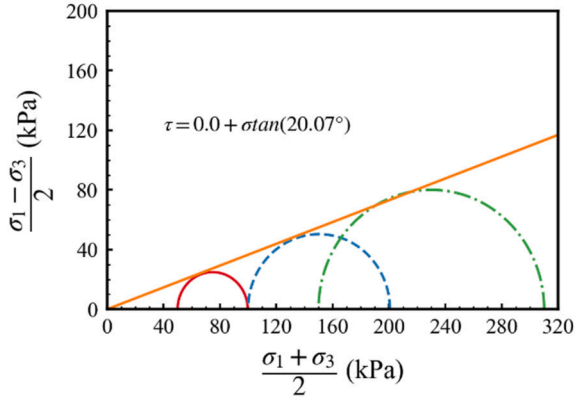

(c) Mohr stress circle of residual strength

Fig. 17. Strain – stress curve and Mohr stress circles of DEM pure fine particle samples.

The motion of the block on the inclined frictional plane can be described by Newton's second law, and its velocity and displacement along the plane with time obey Eqs. (40) and (41), respectively.

$$v_{tangent} = (g\cdot\sin\theta - \mu\cdot g\cdot\cos\theta)\cdot t \tag{40}$$

$$s_{tangent} = \frac{(g\cdot\sin\theta - \mu\cdot g\cdot\cos\theta)\cdot t^2}{2} \tag{41}$$

where g is the vertically downwards acceleration, θ is the dip angle of the inclined plane and μ is the friction coefficient of the plane.

Different configurations of the block are given in Fig. 11, and curves of the velocities and displacement with time are shown in Fig. 12. The simulation results agree well with the analytical solutions for both cases. Both the linear increase in velocity and parabolic increase in displacement can be effectively described by the MPM-DEM method.

To quantitatively illustrate the accuracy of this coupling scheme, a detailed comparison of the maximum velocities and displacements under different friction coefficients is shown in Fig. 13. The errors of the velocities in all of these cases are all less than 0.3%, and the errors of displacement are all less than 0.06%, which shows the reliability of this scheme. Moreover, it is found that the error is less when the block is treated as a DEM particle, which can provide a reference for the chosen modelling schemes to ensure the simulation accuracy.

4. Comparative studies between the MPM-DEM and DEM

4.1. Validation of binary granular mixture triaxial tests

Before applying the proposed MPM-DEM method to soil-rock mixture problems, a comparative study between this method and the pure DEM is described in this section. As a simplification of the soil-rock mixture, a binary granular mixture is chosen to verify the correctness of the MPM-DEM as a benchmark example. In the binary granular mixture, the particles are divided into coarse particles and fine particles, and the gradation is discontinuous (Zhou et al., 2018), which makes it easy to implement numerically.

A set of binary granular mixture samples for triaxial tests with a particle size ratio of 1:10 under different coarse particle contents and confining pressures is generated and simulated using a pure DEM code. The particle size ratio refers to the ratio between the mean size of the fine particles and the mean size of the coarse particles, and it is introduced to describe the gradation. The mean particle sizes are set to 0.01 m and 0.001 m for coarse and fine particles, respectively. The coarse particle content, which is called the rock content in soil-rock mixture problems, is measured by the percentage of the mass of coarse particles in the sample, and three levels of 0%, 20%, and 40% coarse particle contents are considered in this section. First, a series of triaxial tests are carried out under a confining pressure of 50 kPa for each sample, and two additional confining pressures of 100 kPa and 150 kPa are then implemented using the 0% coarse particle content sample for macro-parameter calibration for the MPM-DEM simulation. In addition, a uniformly distributed gradation in the range of 0.95 to 1.05 times the preset particle size is introduced for fine and coarse particles to avoid crystallization. Fig. 14 shows the particle grading curves of different samples.

The volume expansion method, which is widely-used in DEM simulations, is used in conjunction with our ghost radius calculating scheme to generate the triaxial samples. First, particles with diameters 1/5 times the target grain size are generated in a domain slightly larger than the sample size. Then, the diameters of the particles expand to the target grain size at a very slow rate. After the expansion process, the samples are compacted until the preset confining pressure is reached for triaxial tests. By adopting this method, reasonable initial overlaps can be obtained in the numerical models, which ensures the samples are established at a correct initial stress state. Samples with a side length of approximately 0.075 m are generated under different confining pressures, and the number of particles in each sample is presented in Table 2. Three of the samples with coarse particle contents of 0%, 20% and 40% under a confining pressure of 50 kPa are depicted in Fig. 15.

First, three triaxial tests of different coarse particle contents under a

Table 3
Macro-parameters of fine particles in binary granular mixtures.

Density (kg/m^3)	Young's modulus (MPa)	Poisson's ratio	Peak cohesion (Pa)	Residual cohesion (Pa)	Peak friction angle (°)	Residual friction angle (°)	Dilatancy angle (°)
Determined by porosity of each sample	4.6	0.12	0.0	0.0	28.6	18.6	16.0

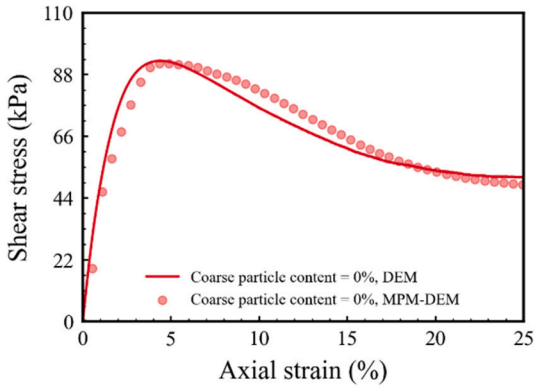

Fig. 18. Curves of MPM-DEM pure fine particle samples under 50 kPa confining pressure.

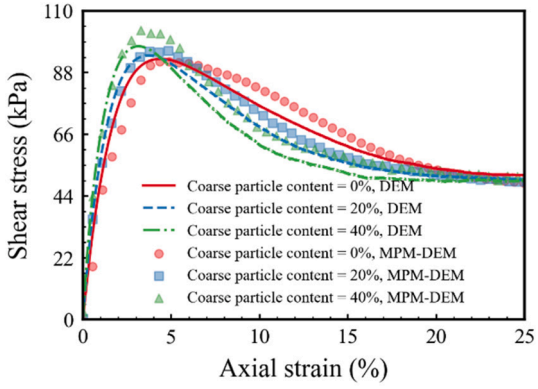

Fig. 19. Results of the MPM-DEM under different coarse particle contents.

confining pressure of 50 kPa are carried out using the pure DEM to explore the influence of the coarse particle content on mechanical behaviours. The micro-parameters used in the pure DEM simulations are as follows: the Young's modulus of the fine and coarse particles are both set as 0.8 GPa, the Poisson's ratios are both set to 0.12, and the densities are both selected as 2600.0 kg/m^3. The friction coefficients between fine particles, between coarse particles and between fine particles and coarse particles are all set to 0.35. The loading velocity is set to 0.002 m/s, which satisfies the requirement of the inertia index (Jop et al., 2006), as shown in Eq. (42). The time interval is set to 1.0e-6 s, and a total of 6.4 million steps have been simulated.

$$I = \dot{\varepsilon}\cdot\overline{d}\cdot\sqrt{\frac{\rho}{P}} \leqslant 10^{-3} \tag{42}$$

where $\dot{\varepsilon}$ is the axial strain rate, $\overline{d}$ is the mean grain size of the sample, ρ is the density and P is the confining pressure.

As shown in Fig. 16, the axial strain-shear stress curves of the samples under 50 kPa confining pressure present a trend of hardening first and softening thereafter. The peak shear stress increases with increasing coarse particle content, while the residual shear stresses are shown to be the same independent of the coarse particle content. It is also found that the hardening and softening phenomena become faster with increasing coarse particle content.

In the MPM-DEM scheme, the fine particles are simulated by the MPM, and macro-parameters of a set of fine particles are thereby needed. Two additional triaxial tests involving pure fine particle samples under 100 kPa and 150 kPa confining pressures are then carried out using the DEM. The axial strain – shear stress curves of these tests are shown in Fig. 17(a).

The cohesion and friction angle of fine particles can be determined by the Mohr stress circles, as shown in Fig. 17(b) and (c). In addition, Young's modulus and the dilatancy angle are determined by the result of fine particles under a 50 kPa confining pressure. All of the macro-parameters for the simulation are summarized in Table 3. It should be noted that the friction angle and cohesion are slightly lower than those obtained from the Mohr circles because the outer circle of the Drucker-Prager yield surface is used in this simulation. These macro-parameters remain unchanged in the following MPM-DEM simulations and are not affected by the coarse particle content.

To describe the phenomenon of the hardening and softening behaviour shown in the pure fine particles, a cubic hardening function and an exponential softening function are introduced in Eq. (43), which is expressed as follows:

$$\varphi = \begin{cases} \varphi_e, & \varepsilon_p = 0 \\ a\varepsilon_p^3 + b\varepsilon_p^2 + c\varepsilon_p + d, & 0 < \varepsilon_p \leqslant \varepsilon_p^{peak} \\ \varphi_r + (\varphi_p - \varphi_r)e^{-H\left(\varepsilon_p - \varepsilon_p^{peak}\right)}, & \varepsilon_p > \varepsilon_p^{peak} \end{cases} \tag{43}$$

where ε_p is the cumulative equivalent plastic strain at the current time, ε_p^{peak} is the cumulative equivalent plastic strain when the shear stress reaches the peak value and is set to 0.022 in this work, φ_r and φ_p are the residual friction angle and peak friction angle, respectively, and φ_e is the friction angle used in the elastic stage, which is chosen to be the same as φ_r in this simulation. a, b, c, and d are the coefficients of the hardening function, which are set to 1075.64, −407.93, 16.39 and 0.32, respectively. H is a coefficient related to the softening rate and is set to 50.0 here.

To incorporate the constitutive model, a pure MPM triaxial test under 50 kPa is simulated using the proposed MPM-DEM method. The fine-particle sample used in the DEM simulation is used directly to construct the MPM model to obtain an initial overlap between the material points and loading plates to maintain the same confining pressure as the pure DEM test. The result is shown in Fig. 18, where the DEM result is also provided as a comparison. It can be seen from the figure that the result of the MPM-DEM is in good agreement with the DEM result, which indicates that our constitutive model can effectively describe complex soil behaviour, including both the hardening and softening processes. Therefore, the effectiveness of the proposed MPM-DEM method can be preliminarily demonstrated, and the idea of replacing DEM particles with material points is shown to be reliable in successfully capturing soil behaviours. Thereafter, two triaxial tests with coarse particle contents of 20% and 40% are also simulated using the MPM-DEM with the above macro and micro-parameters under a confining pressure of 50 kPa, and the results are shown in Fig. 19.

It can be seen from the figure that the MPM-DEM results are consistent with the DEM solutions. The hardening and softening phenomenon at different coarse particle content levels can be effectively described. Moreover, the influence of the coarse particle content on the peak shear stress and the rate of hardening and softening discovered in the DEM simulations can also be effectively reproduced. In summary,

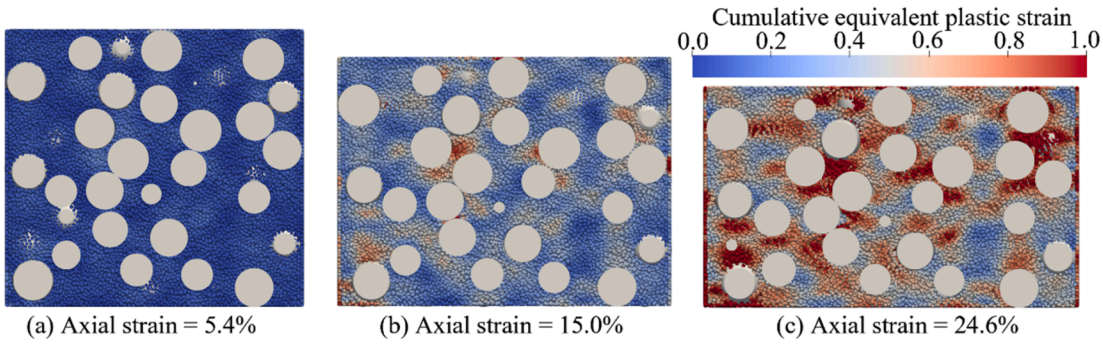

Fig. 20. The plastic zone of 1:10 particle size ratio sample under 60% coarse particle content.

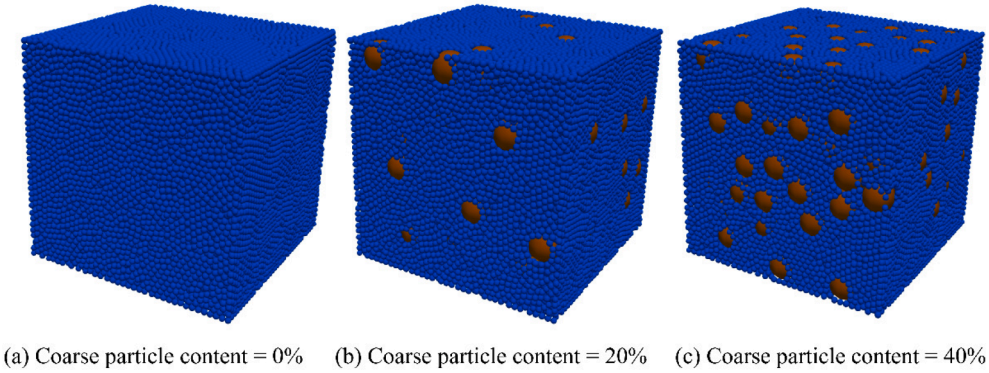

Fig. 21. Coarse-graining MPM-DEM samples with a particle size ratio of 1:5.

the mechanical behaviour of the complex mesoscale system composed of coarse and fine particles can be effectively captured by our method. Therefore, the MPM-DEM is demonstrated to be reliable in the simplest soil-rock mixture problem, that is, the binary granular mixture problem.

Fig. 20 showcases the failure process of the sample containing 60% coarse particles. Evidently, plastic strain accumulates in the vicinity of the rocks, especially in denser regions, as observed in prior studies on soil-rock mixtures (Gong and Liu, 2017; He et al., 2021). From the continuous perspective, this phenomenon results from the high strength of rocks, which limits plastic zone propagation and leads to strain accumulation around the rocks. From the discrete perspective, the area around the rocks is more prone to non-woven deformation. It is worth noting that the sparse distribution of material points around several rocks in Fig. 20 is not caused by contact gaps, but rather by the perspective chosen when creating the cross-sectional view in the post-processing software.

4.2. A coarse-graining modelling scheme based on the MPM-DEM

As mentioned in Section 4.1, a small-sized triaxial test using a DEM simulation with a large particle ratio of 1:10 will result in millions of particles. The computational cost is extremely high, and only super-computing clusters can be used. Coarse-graining modelling scheme is a widely-used simplification technique in DEM simulations to tackle the large particle size ratio problem, where a set of small size particles is replaced by one large size particle. Likewise, in our simulation, we applied this technique to the MPM part. Due to the ghost radius assigned to each MPM particle, it basically inherits both the MPM and DEM particles characteristics. When the contact force is calculated, it behaves as a DEM particle; while for updating the stress and strain of the soils, it acts following the continuum mechanics. Therefore, akin to increasing the mesh size in FEM, coarse-graining modelling scheme in the MPM part essentially refers to the increase of MPM particle size, so that the computational efficiency can be improved as the number of MPM particles is reduced. By doing so, it can eliminate the need for an excessive number of particles, given the condition that the stress state within the continuum part is correct, thereby making the modelling more efficiently. The benefit of this coarse-graining modelling scheme is particularly noticeable when the particle size ratio is extremely large.

To demonstrate the effect of the coarse-graining scheme, a series of coarse-graining MPM-DEM triaxial samples with a particle size ratio of 1:5 (Fig. 21) are generated to reproduce the results of the pure DEM under the particle size ratio of 1:10 simulated in Section 4.1. The constitutive model and the parameters used here are the same as those in Section 4.1. The information of these triaxial tests is presented in Table 4, where the particle reduction scale is introduced to describe the simplified degree of a sample, which is defined as the ratio of the total number of particles between the current sample and the corresponding sample with a 1:10 particle size ratio. As shown in Table 4, the particle reduction scale of these samples is approximately 1:8, that is, approximately 8 fine particles are replaced by one material point in the coarse-graining models.

Table 4
Information on the coarse-graining MPM-DEM triaxial samples.

Sample number	Particle size ratio	Coarse particle content	Confining pressure	Number of material points	Number of coarse DEM particles	Total number of particles	Particle reduction scale
1	1:5	0%	50 kPa	64,000	0	64,000	1:8
2	1:5	20%	50 kPa	53,884	114	53,998	1:8
3	1:5	40%	50 kPa	40,773	224	40,997	1:8

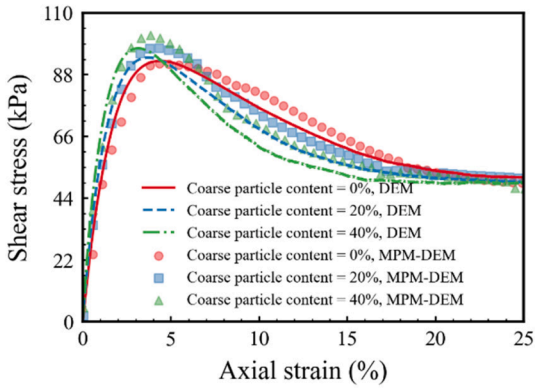

Fig. 22. Results of the MPM-DEM with a particle size ratio of 1:5.

The results under each coarse particle content are depicted in Fig. 22. The mechanical characteristics of hardening and softening can be effectively described with the coarse-graining MPM-DEM samples. Moreover, the influence of the coarse particle content on the peak shear stress and the rate of softening and hardening can also be effectively reflected. The mechanical behaviour of binary mixtures can still be effectively described even if there are fewer particles in the simplified samples, indicating that our simplification with a particle reduction scale of 1:8 is within a reasonable range. Considerable computational resources are saved by this simplification. There is no doubt that the results under a 1:5 particle size ratio with a particle reduction scale of 1:8 are reliable, which means that at least 87.5% of the computational resources can be saved. In fact, the contacts between fine particles do not need to be handled in the MPM-DEM, and the time interval can be increased by using a larger material point size; foreseeably, far more than 87.5% of the computational cost can be reduced.

In addition, the failure process depicted in Fig. 23 demonstrates that the sample with a particle size ratio of 1:5 accurately reproduces the same failure mode observed in the sample with a particle size ratio of 1:10, further validating its accuracy.

Finally, factors affecting the time cost are analysed detailly. As shown in Table 5, A high content of coarse particles generates more ghost particles, resulting in a higher number of contact pairs and elongated pair time. However, the pair time only accounts for a small proportion of the computational time (lower than 20% in tested samples). The other process, including MPM calculation and neighbor list construction times are more time-consuming, which may significantly decrease with smaller number of fine particles. Therefore, the total time cost decrease with higher coarse particle content due to the decrease in total number of particles, indicating that higher coarse particle content does not reduce the computational efficiency of our proposed method.

Based on the MPM-DEM method, a coarse-graining modelling scheme is proposed in this section; this approach is a computational resource-conserving scheme that can greatly increase the efficiency. Its ability to solve the large particle size ratio problem is validated using a series of coarse-graining simplified triaxial tests of binary granular mixtures, which indicates that this method can be used to simulate soil-rock mixture problems.

5. Reproduction of the mechanical behaviour of soil-rock mixtures

To further illustrate the feasibility of the application of this method to soil-rock mixture problems, a series of laboratory medium-sized triaxial tests with 50% rock content implemented by Fan et al. (Fan et al., 2014) are simulated in this section. The rocks used in these triaxial tests are pebbles and gravel, and the soil mass is low liquid limit clay with sand. Three types of samples with rock sizes of 0.005–0.010 m, 0.010–0.016 m and 0.016–0.020 m are constructed and compressed under confining pressures of 200 kPa, 400 kPa and 800 kPa, respectively. The gradations of the samples are presented in Table 6.

Cylindrical samples were directly prepared in a triaxial pressure chamber with dimensions of 0.101 m × 0.2 m (diameter × height). First, the sample was consolidated to the specified confining pressure, and then, an axial displacement boundary condition was applied to begin the triaxial test.

To simulate these triaxial tests, the particle size of the soil particle should be set to at least 1.0e-3 m for the pure DEM, which may result in a large computational cost. However, in the MPM-DEM method, the coarse-graining modelling scheme based on MPM-DEM mentioned in Section 4.2 can be used to increase the size of the material points. In this

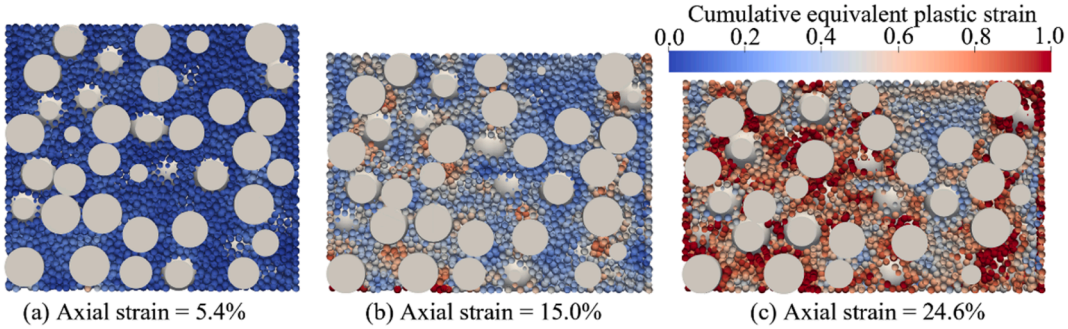

Fig. 23. The plastic zone of 1:5 particle size ratio sample under 60% coarse particle content.

Table 5
Time costs of triaxial tests.

Sample number	Coarse particle content	Number of material points	Number of ghost particles	Pair time (CPU)	Total time (CPU + GPU)
1	0%	64,000	0	0 s	34951 s
2	20%	53,884	6978	3428 s	33160 s
3	40%	40,773	12,257	6022 s	29119 s

Note: The MPM code runs on the GPU (NVIDIA 3060Ti GPU), while DEM is calculated on the CPU (Intel @ Xeon (R) W-2133CPU @ 3.60 GHz CPU) using single core.

Table 6
The gradation of the physical triaxial samples.

Grain Size (m)	Gradation 1	Gradation 2	Gradation 3
0.016–0.020	50%	0%	0%
0.010–0.016	0%	50	0%
0.005–0.010	0%	0%	50%
0.5e-3–1.0e-3	0.6%	0.6%	0.6%
0.25e-3–0.5e-3	1.3%	1.3%	1.3%
0.075e-3–0.25e-3	14.1%	14.1%	14.1%
< 0.075e-3	34.0%	34.0%	34.0%

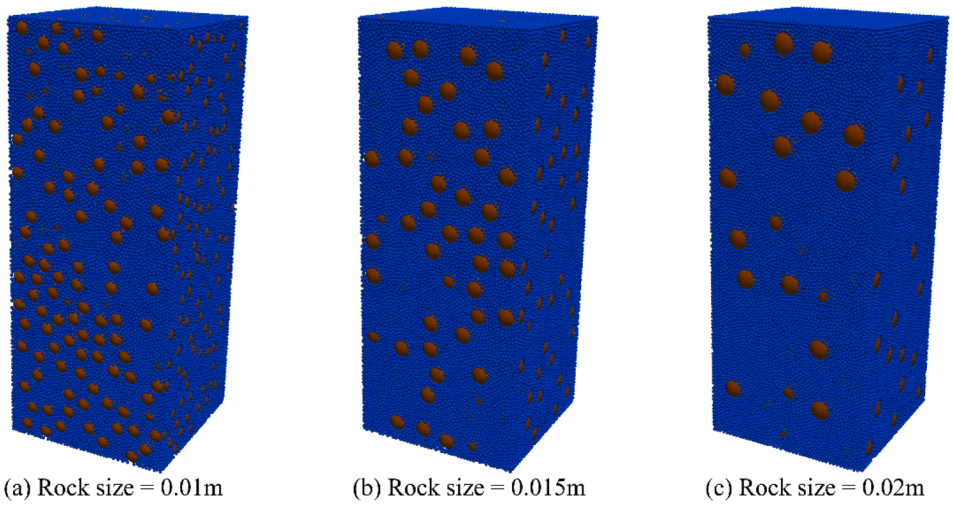

Fig. 24. MPM-DEM models of the laboratory medium-sized triaxial tests.

Table 7
The numbers of particles of different MPM-DEM soil-rock mixture samples.

Rock size	Particle size ratio	Number of material points	Number of coarse DEM particles	Total number of particles
0.010 *m*	1:5	185,505	1486	186,991
0.015 *m*	1:7.5	186,540	451	186,991
0.020 *m*	1:2	186,793	199	186,992

section, the size of the material points is set to 2.0e-3 m, which is two times the maximum grain size of the soil particles. The sizes of the numerical models are slightly different from those of the tests, which are modelled as cuboid with a size of 0.1 m × 0.1 m × 0.2 m to facilitate the application of the boundary conditions, as shown in Fig. 24. In other words, we used a true triaxial stress state to represent a biaxial stress state, which ensures the reliability of our simulated mechanical behaviour. A characteristic particle size method proposed by Du et al. (Du et al., 2017) is used here to simplify the MPM-DEM models; in this method, the diameter of rocks in the range of 0.005–0.010 m is replaced by the characteristic particle size of 0.010 m. Similarly, rocks in the ranges of 0.010–0.016 m and 0.016–0.020 m are treated in the same way, with characteristic particle sizes of 0.015 m and 0.020 m, respectively. Similar to the triaxial tests of binary granular mixtures, the volume expansion method is used to generate the numerical samples. The numbers of particles in samples with different rock sizes are listed in Table 7.

Using the proposed MPM-DEM method, the soil mass is treated as a set of material points with macro-parameters, and the rocks are treated as DEM particles with micro-parameters. The macro-parameters of the soil used in the simulation are listed in Table 8 for clarity. The micro-parameters of the rock are set as follows: the density is 2700 kg/m3, the Young's modulus is 50 GPa and Poisson's ratio is 0.20, referred from the work of Du et al. (Du et al., 2017). Because the micro-parameters of a single soil particle are not mentioned in related studies on this test, the micro-parameters of the soil particle are assumed to be the same as those of the rock for simplicity. The interaction between rock or rock-soil particles is considered purely frictional, and the cohesion effect is neglected. The interparticle frictional coefficient between the rock and rock-soil contacts is 0.3. The Drucker-Prager yield criterion and a linear hardening function are used here to describe the hardening phenomenon in the triaxial tests.

The simulation results of the MPM-DEM are presented in Fig. 25 and compared with the results from the tests. The simulation results under different confining pressures and rock sizes are generally consistent with the test results. The difference between simulations and tests can be explain as the samples in simulations cannot be exact as in tests. Regardless, these results demonstrate the potential of our approach to address soil-rock mixture problems with a reasonable accuracy.

Moreover, by analysing the curves for different rock sizes, it can be easily discovered that the influence of rock size can be effectively captured by the proposed MPM-DEM method. The axial strain – shear stress curves are typical hardening curves without obvious peak values. The mechanical behaviour is greatly affected by the rock size; with increasing rock size, the peak value decreases, and the hardening phenomenon becomes more obvious, especially under higher confining pressure. This phenomenon means that the influence mechanism of rock size on the mechanical characteristics of soil-rock mixtures has been correctly reflected.

As shown in Fig. 26, the plastic zone distributions at different time steps reveal that the primary driver of soil failure lies in the substantial plastic deformation within the zone containing dense rocks. Ultimately, the connected plastic zones culminate in the formation of a shear zone, which triggers sample failure.

In summary, the MPM-DEM is a suitable method for simulating soil-rock mixtures. It can effectively reproduce and predict mechanical behaviour, especially the influence of rock size. Therefore, it is a reliable method and can be applied to soil-rock mixtures.

Table 8
The macro-parameters of soil used in the MPM-DEM simulation.

Confining pressure (kPa)	Density (kg/m^3)	Young's modulus (MPa)	Poisson's ratio	Cohesion (kPa)	Friction angle (°)	Dilatancy angle (°)
200 kPa 400 kPa 800 kPa	Determined by the porosity of each sample	3.0 4.8 8.5	0.3	Linear Hardening from 20.5 kPa	Linear Hardening from 30.0°	5.0

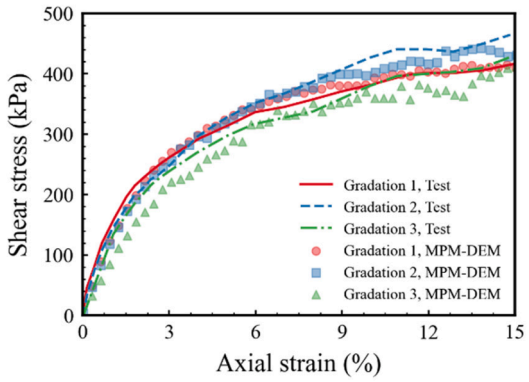

(a) Confining pressure = 200 kPa

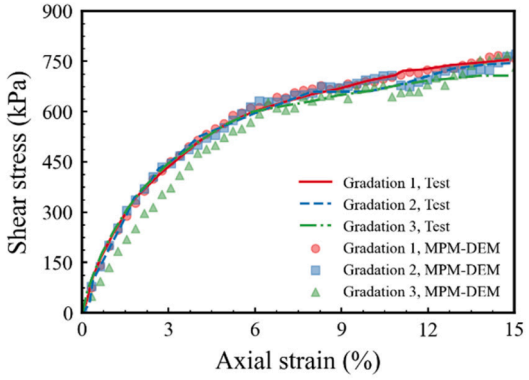

(b) Confining pressure = 400 kPa

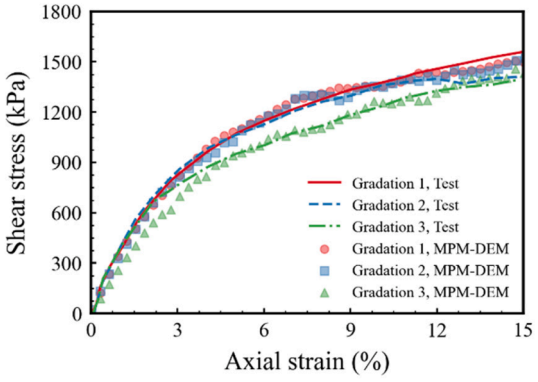

(c) Confining pressure = 800 kPa

Fig. 25. Axial strain – shear stress curves under different confining pressures.

6. Discussions

It is worth noting that the proposed MPM-DEM coupling method does have constraints and limitations in some circumstances. When the models are oversimplified using the coarse-graining modelling scheme, the simulation results become distorted. Following the study in Section 4.1, the models with a particle size ratio of 1:10 are further simplified to a particle size ratio of 1:2.5, as shown in Fig. 27. One material point in these models represents approximately 64 fine particles, and the triaxial tests are carried out under the same conditions mentioned in Section 4.1.

As shown in Fig. 28, the hardening and softening phenomenon, the trend of peak shear stress and the rate of hardening and softening increasing with the coarse particle content can still be effectively described. However, the errors of the peak shear stresses are significantly higher, especially under higher coarse particle contents. A possible reason for this phenomenon is that when the size of the material points is too large, the flow of material points in the gap between the coarse DEM particles is blocked, and the coarse-graining simplified model can no longer describe its mechanical behaviour. Another reason may be that the coupling contact force in the MPM is calculated on the material points first and then mapped to the grid nodes to solve the governing equations thereafter. The coupling contact force on a grid node is the summation of its neighbour particle list, which is different from the initial coupling force on material points. Because of this difference, errors may occur when reflecting the mechanical behaviour of the soil-rock interaction, especially when the background mesh is very coarse.

Another limitation is that the proposed MPM-DEM scheme may lose accuracy in soil-rock mixtures with large coarse particle contents. The premise of using material points with a continuum constitutive model to describe the mechanical behaviour of fine particles is that there are a sufficient number of fine particles in the gap between coarse particles, so the soil shows the characteristics of continuum media.

Basically, our MPM-DEM method is proposed mainly for solving soil-rock mixtures with large particle size ratios. Compared to the traditional DEM simulations, it has advantages of computational efficiency because the fine particles are treated as a continuum. So far, to our experience, we have found that the accuracy can be guaranteed when the particle size ratio is greater than 1:5. This is because when the particle size ratio is larger, the tracking of the contact boundary is more accurate. However, two things are worthy to be mentioned. 1) When particle size ratio is very large, computational resources will be still very high, causing a great many of particles in the system. That is also the reason we incorporate the coarse-graining scheme for reducing the number of MPM particles. 2) When dealing with small particle size ratios (less than 1:5) and exceedingly high rock contents, the reliability of our method may degrade, and in these situations, using a pure DEM modelling scheme may be more appropriate.

7. Conclusions

In this paper, a coupled MPM-DEM method is proposed to simulate soil-rock mixtures with large particle size ratios. The soil particles are treated as material points, while the rocks are treated with the DEM. To calculate the coupling contact force, that is, the linking of the MPM-DEM method, a scheme based on ghost particles is introduced. Moreover, a coarse-graining modelling scheme based on the MPM-DEM is proposed to model soil using fewer material points with larger particle sizes. By using this scheme, the number of particles can be greatly reduced, and the time interval can be further increased, which significantly reduces the computational cost during simulation.

Four examples are introduced in this paper to validate this method. The accuracy of the normal contact and tangential contact model are first proven by the ball impacting example and the block sliding example. Then, a series of triaxial tests of binary granular mixtures are simulated using both the same models as pure DEM simulations and coarse-graining simplified models. The results indicate that the MPM-DEM method can reproduce the results of the pure DEM under the same numerical model and can effectively describe the mechanical behaviour of materials with a large particle size ratio using the coarse-graining modelling scheme. Finally, a series of laboratory triaxial tests of soil-rock mixtures are simulated to prove the validity of this method. The results show that the mechanical behaviour of soil-rock mixtures can also be effectively described, and the influence of rock size is also captured. In summary, the proposed MPM-DEM method is an efficient and accurate method for solving soil-rock mixture problems, and it also has broad prospects in other fields of geotechnical engineering.

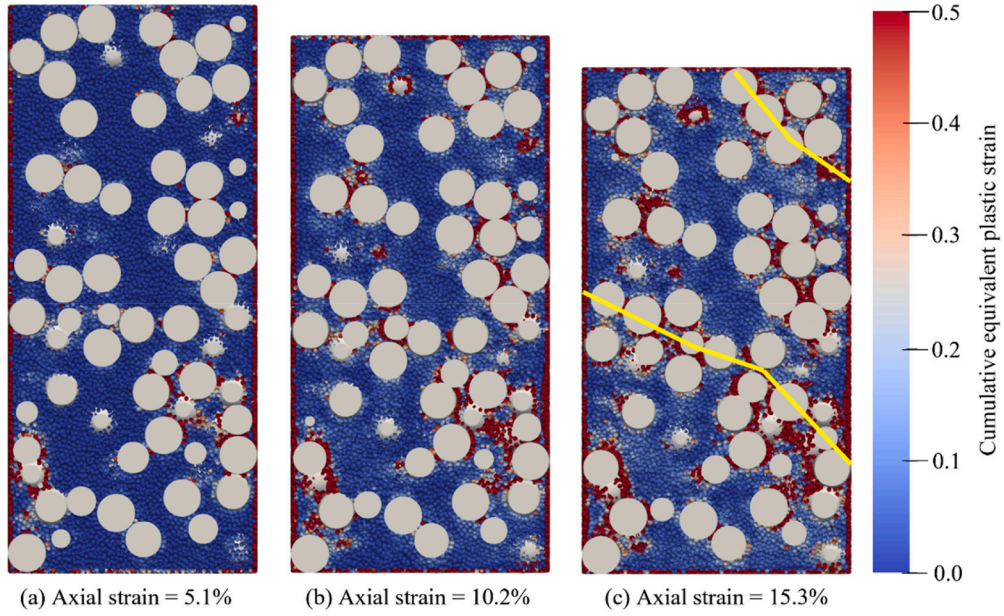

Fig. 26. Cumulative equivalent plastic strain of Gradation 2 under 800 kPa confining pressure.

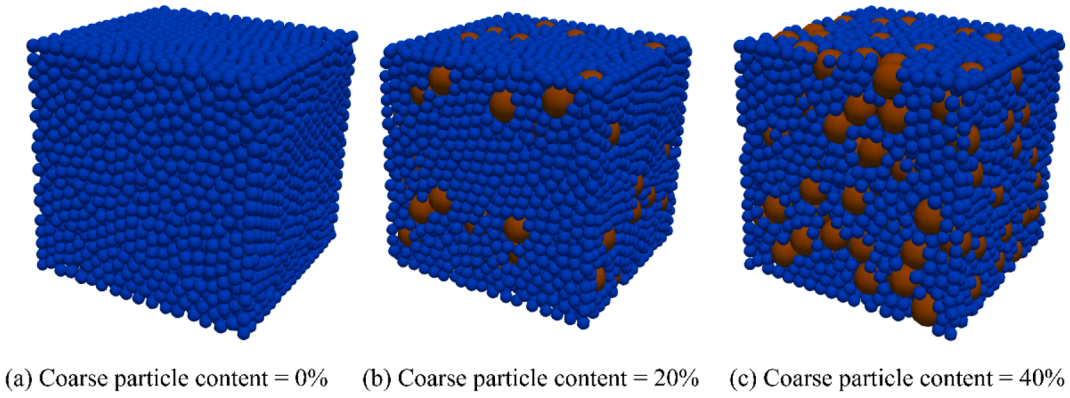

Fig. 27. Binary granular samples of the MPM-DEM with a particle size ratio of 1:2.5.

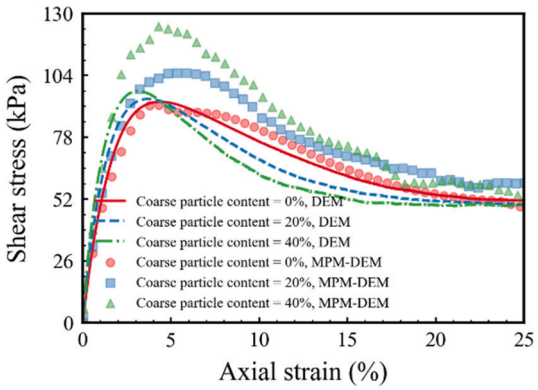

Fig. 28. Results of the MPM-DEM for a particle size ratio of 1:2.5.

CRediT authorship contribution statement

Jianguo Li: Methodology, Software, Validation, Formal analysis, Data curation, Visualization, Writing – original draft, Writing – review & editing. **Bin Wang:** Conceptualization, Methodology, Writing – review & editing, Supervision, Funding acquisition. **Di Wang:** Methodology, Software, Writing – review & editing, Supervision. **Pei Zhang:** Methodology, Writing – review & editing. **Philip.J Vardon:** Formal analysis, Writing – review & editing.

Declaration of Competing Interest

The authors declare that they have no known competing financial interests or personal relationships that could have appeared to influence the work reported in this paper.

Data availability

Data will be made available on request.

Acknowledgements

The authors wish to acknowledge the National Natural Science Foundation of China (Grant Nos. 51979270 and 51709258) and the CAS Pioneer Hundred Talents Program for their financial supports.

References

Berzins, M., 2022. Energy conservation and accuracy of some MPM formulations. Comp. Part. Mech. 9, 1205–1217.

Brackbill, J.U., Kothe, D.B., Ruppel, H.M., 1988. Flip: A low-dissipation, particle-in-cell method for fluid flow. Comput. Phys. Commun. 48, 25–38.

Brackbill, J.U., Ruppel, H.M., 1986. FLIP: A method for adaptively zoned, particle-in-cell calculations of fluid flows in two dimensions. J. Comput. Phys. 65, 314–343.

Cen, W., Luo, J., Yu, J., Shamin, R.M., 2020. Slope Stability Analysis Using Genetic Simulated Annealing Algorithm in Conjunction with Finite Element Method. KSCE J. Civ. Eng. 24, 30–37.

Chen, Y.C., Mayte, C., Yue, Y., Eita, G., Ken, K., 2021. Hybrid Discrete-Continuum Modeling of Shear Localization in Granular Media. J. Mech. Phys. Solids 153, 104404.

Dong, Y., Grabe, J., 2018. Large scale parallelisation of the material point method with multiple GPUs. Comput. Geotech. 101, 149–158.

Du, X., Zhang, P., Jiu, L., 2017. A mesoscopic equivalent analysis method for the study on macro mechanical properties of soil-rock mixture. Eng. Mech. 34, 44–52 [in Chinese].

Dyson, A.P., Tolooiyan, A., 2019a. Prediction and classification for finite element slope stability analysis by random field comparison. Comput. Geotech. 109, 117–129.

Dyson, A.P., Tolooiyan, A., 2019b. Probabilistic investigation of RFEM topologies for slope stability analysis. Comput. Geotech. 114, 103129.

Fan, J., Hong, B., Liu, S., Liu, X., 2014. Study on the Effect of Rock Size on Strength Characteristics of Soil-rock Mixture. Sci. Technol. Eng. 14, 268–272 [in Chinese].

Gan, Y., Sun, Z., Chen, Z., Zhang, X., Liu, Y., 2018. Enhancement of the material point method using B-spline basis functions. Int. J. Numer. Methods. Eng. 113, 411–431.

Gao, W., Lu, X., Peng, Y., Wu, L., 2020. A deep learning approach replacing the finite difference method for in situ stress prediction. IEEE Access 8, 44063–44074.

Gong, J., Liu, J., 2017. Influences of rock proportion on failure process and failure mode of soil-rock-mixture slope with PIV analysis. Rock Soil Mech. 38, 696–704 [in Chinese].

Goniva, C., Kloss, C., Deen, N.G., Kuipers, J.A.M., Pirker, S., 2012. Influence of rolling friction on single spout fluidized bed simulation. Particuology 10, 582–591.

He, Y., Zhang, Z., Yang, Q., Zhang, J., Li, W., 2021. Random Generation and Stability Analysis of Soil-rock Mixture Slope Model. South China Geology 37, 226–232 [in Chinese].

Hu, F., Li, Z.Q., Hu, R.L., Zhou, Y.X., Yue, R.Q., 2018. Research on the deformation characteristics of shear band of soil-rock mixture based on large scale direct shear test. Chin. J. Rock Mech. Eng. 37 (3), 766–778 [in Chinese].

Huang, J., Griffiths, D., Fenton, G.A., 2010. System reliability of slopes by RFEM. Soils Found. 50, 343–353.

Iverson, R.M., 1997. The physics of debris flows. Rev. Geophys. 35 (3), 245–296.

Ji, X.P., Han, B., Hu, J.M., Li, S.W., Xiong, Y., Sun, E.Y., 2022. Application of the discrete element method and CT scanning to investigate the compaction characteristics of the soil–rock mixture in the subgrade. Road Mater. Pavement Des. 23, 397–413.

Jiang, Y., Zhao, Y., Choi, C.E., Choo, J., 2022. Hybrid continuum–discrete simulation of granular impact dynamics. Acta Geotech. 17, 5597–5612.

Jop, P., Forterre, Y., Pouliquen, O., 2006. A constitutive law for dense granular flows. Nature 441, 727–730.

Kan, L., Liang, Y., Zhang, X., 2021. A critical assessment and contact algorithm for the staggered grid material point method. Int. J. Mech. Mater. Des. 17, 743–766.

Li, L., Chu, X., 2019. Failure Mechanism and Factor of Safety for Spatially Variable Undrained Soil Slope. Adv. Civ. Eng. 1–17.

Li, J., Wang, B., Jiang, Q., He, B., Zhang, X., Vardon, P.J., 2022. Development of an adaptive CTM–RPIM method for modeling large deformation problems in geotechnical engineering. Acta Geotech. 17, 2059–2077.

Liu C. Q., Sun Q., Gordon G. D. Zhou, 2018. Coupling of material point method and discrete element method for granular flows impacting simulations: Coupling of MPM and DEM for Granular Flows Impacting Simulations. Int. J. Numer. Methods Eng. 115, 172–188.

Luo, G., Zhao, Y., Shen, W., Wu, M., 2022. Dynamics of bouldery debris flow impacting onto rigid barrier by a coupled SPH-DEM-FEM method. Comput. Geotech. 150, 104936.

Nasiri, M., Hajiazizi, M., 2020. The Effects of Strength Parameters on Slope Safety Factor in 2D & 3D Analyses using Numerical Methods. Int. J. Min. Geo. Eng. 54, 71–75.

Navas, P., López-Querol, S., Yu, R.C., Pastor, M., 2018. Optimal transportation meshfree method in geotechnical engineering problems under large deformation regime: OTM in Geotechnical engineering problems under large deformation regime. Int. J. Numer. Methods Eng. 115, 1217–1240.

Ni, A., Ma, G., Zhou, H., Wang, D., Lu, X., Zhou, W., 2022. DEM Investigation of the Microscopic Mechanism of Scale Effect of Sandy Gravel Material. Acta Geotech.

Remmerswaal, G., Vardon, P.J., Hicks, M.A., 2021. Evaluating residual dyke resistance using the Random Material Point Method. Comput. Geotech. 133, 104034.

Ren, S.K., Zhang, P., Galindo-Torres, S.A., 2022. A coupled discrete element material point method for fluid–solid–particle interactions with large deformations. Comput. Method. Appl. M. 395, 115023.

Schuster, R.L., Highland, L.M., 2007. The third hans cloos lecture Urban landslides: Socioeconomic impacts and overview of mitigative strategies. Bull. Eng. Geol. Environ. 66 (1), 1–27.

Serrano-Pacheco, A., Murillo, J., García-Navarro, P., 2009. A finite volume method for the simulation of the waves generated by landslides. J. Hydrol. 373, 273–289.

Singer, V., Sautter, K.B., Larese, A., Wüchner, R., Bletzinger, K.U., 2022. A partitioned material point method and discrete element method coupling scheme. Adv. Model. and Simul. in Eng. Sci. 9, 16.

Trujillo-Vela, M.G., Galindo-Torres, S.A., Zhang, X., Ramos-Cañón, A.M., Escobar-Vargas, J.A., 2020. Smooth particle hydrodynamics and discrete element method coupling scheme for the simulation of debris flows. Comput. Geotech. 125, 103669.

Valiani, A., Caleffi, V., Zanni, A., 2002. Case Study: Malpasset Dam-Break Simulation using a Two-Dimensional Finite Volume Method. J. Hydraul. Eng. 128, 460–472.

Wang D., Wang B., Jiang Q., Guo N., Zhang W., He K. y., 2022. Large Deformation Slope Failure — A Perspective from Multiscale Modelling. Comput. Geotech. 150, 104886.

Wang, D., Jan, C., Zhou, W., Dorostkar, O., 2021. On the Effect of Grain Fragmentation on Frictional Instabilities in Faults With Granular Gouge. J. Geophys. 126.

Wang, B., Li, J., Jiang, Q., Yang, Y.T., Feng, X.T., 2020. An improved FE-Meshfree method for solving steady seepage problems. Comput. Geotech. 119, 103223.

Wang, B., Wang, D., Hicks, M.A., Feng, X.T., 2023. Interplay Between Friction and Cohesion: A Spectrum of Retrogressive Slope Failure. J. Geophys. Res-Sol. Ea. 128 (2).

Wu, S.R., 2006. Lumped mass matrix in explicit finite element method for transient dynamics of elasticity. Comput. Method. Appl. M. 195, 5983–5994.

Xu, W.J., Zhang, H.Y., 2021. Research on the effect of rock content and sample size on the strength behavior of soil-rock mixture. Bull. Eng. Geol. Environ. 80, 2715–2726.

Xu, W.J., Wang, S., Zhang, H.Y., Zhang, Z.L., 2016. Discrete element modeling of a soil-rock mixture used in an embankment dam. Int. J. Rock Mech. Min. 86, 141–156.

Xu, W., Yue, Z., Hu, R., 2008. Study on the mesostructure and mesomechanical characteristics of the soil–rock mixture using digital image processing based finite element method. Int. J. Rock Mech. Min. 45, 749–762.

Yamaguchi, Y., Moriguchi, S., Terada, K., 2021. Extended B-spline-based implicit material point method. Int. J. Numer. Meth. Eng. 122, 1746–1769.

Yang, X., Yang, G., Yu, T., 2012. Comparison of Strength Reduction Method for Slope Stability Analysis Based on ABAQUS FEM and FLAC3D FDM. Appl. Mech. Mater. 170–173, 918–922.

Yao, Y., Li, J., Ni, J., Liang, C., Zhang, A., 2022. Effects of gravel content and shape on shear behaviour of soil-rock mixture: experiment and DEM modelling. Comput. Geotech. 141, 104476.

Ye, G., Zhang, F., Yashima, A., Sumi, T., Ikemura, T., 2005. Numerical analyses on progressive failure of slope due to heavy rain with 2d and 3d fem. Soils Found. 45, 1–15.

Yue Y., Smith B., Y. Peter C., Maytee C., Ken K., Eitan G., 2018. Hybrid Grains: Adaptive Coupling of Discrete and Continuum Simulations of Granular Media. ACM Trans. Graph. 37, 1–19.

Zhang, H.M., Dong, X.H., Li, Z.G., 2001. Study on contact algorithm of dynamic explicit FEM for sheet forming simulation. Wuhan Univ. J. Nat. Sci. 6, 704–708.

Zhao, L.H., Huang, D.L., Zhang, S.H., Cheng, X., Luo, Y.B., Deng, M., 2021. A new method for constructing finite difference model of soil-rock mixture slope and its stability analysis. Int. J. Rock Mech. Min. 138, 104605.

Zhao, S.W., Zhao, J.D., 2019. A Poly-superellipsoid-based Approach on Particle Morphology for DEM Modeling of Granular Media. Int. J. Numer. Anal. Methods Geomech. 43, 2147–2169.

Zhou, W., Wu, W., Ma, G., Ng, T., 2018. Chang X, Undrained behavior of binary granular mixtures with different fines contents. Powder Technol. 340, 139–153.

Zhou, W., Wang, D., Ma, G., Cao, X.X., Hu, C., Wu, W., 2020. Discrete Element Modeling of Particle Breakage Considering Different Fragment Replacement Modes. Powder Technol. 360, 312–323.

Zhu, H., Zhang, L.M., 2013. Characterizing geotechnical anisotropic spatial variations using random field theory. Can. Geotech. J. 50, 723–734.